pubs.acs.org/Biomac

Review

Chitosan as a Canvas for Studies of Macromolecular Controls on $CaCO_3$ Biological Crystallization

Brenna M. Knight, Kevin J. Edgar, James J. De Yoreo, and Patricia M. Dove*

Cite This: *Biomacromolecules* 2023, 24, 1078−1102

Read Online

ACCESS | Metrics & More | Article Recommendations | Supporting Information

Downloaded via VIRGINIA POLYTECH INST STATE UNIV on July 27, 2023 at 17:36:29 (UTC).
See https://pubs.acs.org/sharingguidelines for options on how to legitimately share published articles.

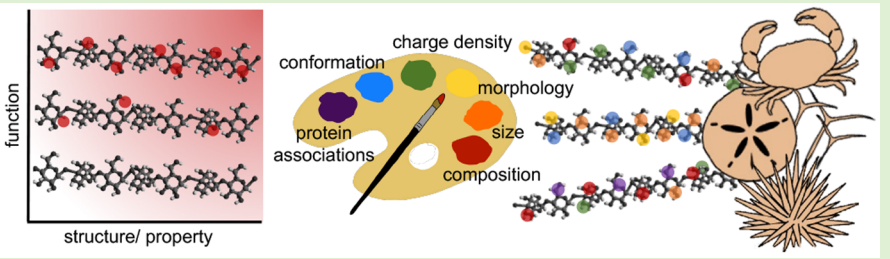

ABSTRACT: A mechanistic understanding of how macromolecules, typically as an organic matrix, nucleate and grow crystals to produce functional biomineral structures remains elusive. Advances in structural biology indicate that polysaccharides (e.g., chitin) and negatively charged proteoglycans (due to carboxyl, sulfate, and phosphate groups) are ubiquitous in biocrystallization settings and play greater roles than currently recognized. This review highlights studies of $CaCO_3$ crystallization onto chitinous materials and demonstrates that a broader understanding of macromolecular controls on mineralization has not emerged. With recent advances in biopolymer chemistry, it is now possible to prepare chitosan-based hydrogels with tailored functional group compositions. By deploying these characterized compounds in hypothesis-based studies of nucleation rate, quantitative relationships between energy barrier to crystallization, macromolecule composition, and solvent structuring can be determined. This foundational knowledge will help researchers understand composition-structure-function controls on mineralization in living systems and tune the designs of new materials for advanced applications.

1. INTRODUCTION

Many living systems produce morphologically complex mineral-organic composites in processes broadly known as biological crystallization, or biomineralization. All phyla contain organisms that can form biominerals, but the ability of animals in the Opisthokonta clade, which includes fungi and amoebae organisms, to produce mineralized structures is of particular interest.[1] More than 60 inorganic phases have been identified with most biominerals formed by animals composed of calcium carbonate ($CaCO_3$), calcium phosphate, or silica (Figure 1).[2−6] Organisms have evolved roles for biominerals that go well-beyond skeletal support to include functions such as filtration, grinding, cutting, light harvesting, gravity sensing, and magnetic guidance.[1,7]

The predominant $CaCO_3$ polymorphs—calcite and aragonite—have particular significance in environmental chemistry due to their influence on global climate through the biogeochemical capture of carbon into inorganic and biogenic reservoirs.[8−11] Owing to the ecological diversity of animals that produce $CaCO_3$, it is unsurprising their biominerals display arguably the highest structural variability of all functional biomaterials (Figure 2). These mineral-reinforced structures confer critical advantages for animal survival, including predation, motility, and reproduction.[1,7] For example, the predator-resistant $CaCO_3$-organic shells of mollusks from the genus *Haliotis* have a fracture resistance that is a thousand times stronger than their inorganic mineral component alone (aragonite).[12,13]

The fidelity and hierarchical organization of biomineral structures have inspired an extensive effort to understand the processes by which biomolecules direct crystal nucleation and growth during mineralization. Central to controlled mineralization is the organic matrix of macromolecules that constitutes the local setting where amorphous and crystalline phases are formed. Broadly defined, the organic matrix is a gel-like mixture of proteins, polysaccharides, proteoglycans of variable sugar/protein ratios, and lipids.[14−25] Investigators are increasingly identifying new roles for the organic matrix including concentrating precursor ions, providing substrates that direct the location and preferred orientation of nucleated crystals, and controlling the crystal polymorph that forms.[17,23,26−30]

Received: November 22, 2022
Revised: January 26, 2023
Published: February 28, 2023

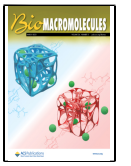

© 2023 American Chemical Society

https://doi.org/10.1021/acs.biomac.2c01394
Biomacromolecules 2023, 24, 1078−1102

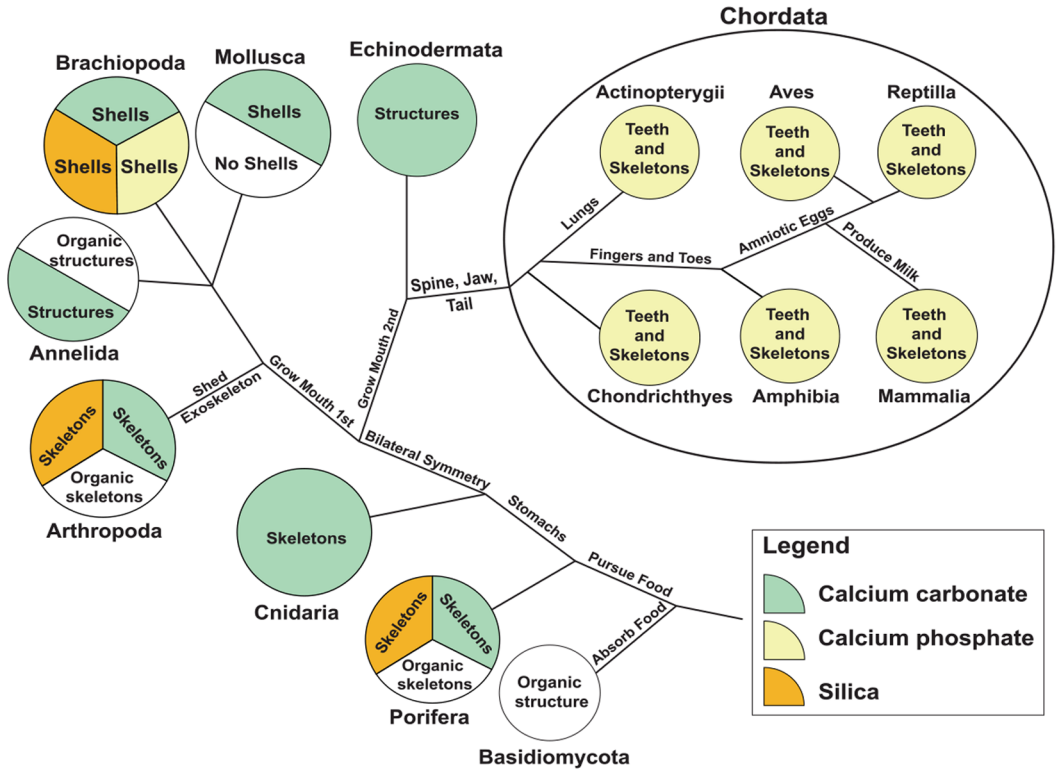

Figure 1. Illustration of the general phylogenetic relations for modern animals in the Opisthokonta clade and the most common classes of biominerals produced by each group. Marine organisms produce predominantly polymorphs of $CaCO_3$, and calcium phosphates are formed by the chordates (animals with vertebrae). Silica biominerals have ecological significance but relatively minor species diversity in the modern ocean, (after S. Mergelsberg, unpublished).

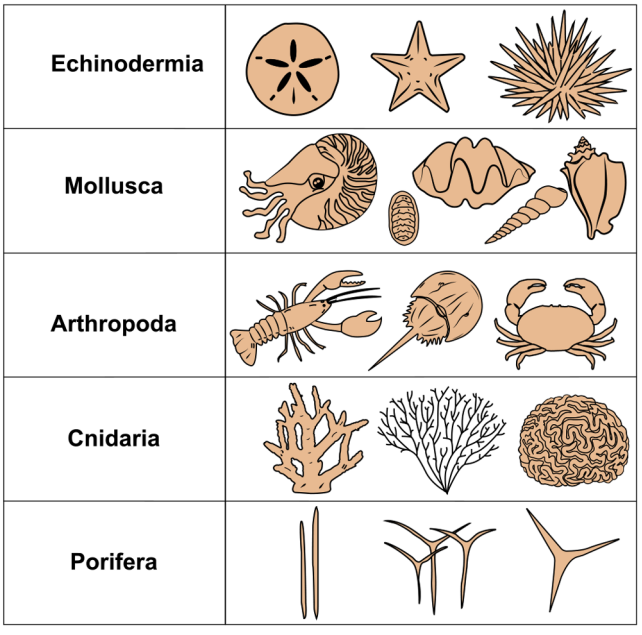

Figure 2. Examples of skeletal structures with identified polysaccharide-biomineral associations. Echinoderms produce structures with high diversity. The Mollusca are the largest phylum of animals and have received much attention for the morphological and functional diversity of their biomineral structures. Arthropoda are defined in part by their chitin cuticle that can be reinforced by $CaCO_3$ to produce biocomposites with remarkable fracture toughness.[12,93,96] The Cnidarians and Porifera also have polysaccharide-mineral associations, particularly in corals and marine sponges, respectively.

However, despite considerable efforts, we still lack an understanding of how the structure and composition of these macromolecular assemblages direct crystal formation and the subsequent growth and transformation processes to final products.

In this review, we show how recent insights into the composition of the organic matrix, combined with advances in glycomaterials, provide a transformational opportunity to establish the physical basis for macromolecular controls on biomineralization. First, we highlight primary constituents of the organic matrix and the analytical challenges that have shaped traditional models. We then discuss recent studies documenting the ubiquitous presence of polysaccharides and glycoproteins at sites of calcification. The emerging picture is that natural glycomaterials are enriched in carboxyl and sulfate groups, comparable to the acidic character of proteins. We then examine studies of $CaCO_3$ crystallization onto chitin and other chitinous materials. Most of these studies are highly qualitative and the materials not well-characterized; characterization of structurally complex, variable polysaccharides and derivatives is crucial and challenging. The available evidence, however, indicates the overarching influence of functional group properties, not molecular class, upon crystallization. Finally, we suggest that recent advances in natural polymer chemistry enable novel hypothesis-based studies of macromolecular controls on mineral crystallization. We discuss chitosan, a synthetically deacetylated chitin, as a promising and versatile material that can be derivatized for systematic, quantitative studies to establish kinetic and thermodynamic drivers to mineralization. This understanding will make it possible to build conceptual and computational models that

https://doi.org/10.1021/acs.biomac.2c01394
Biomacromolecules 2023, 24, 1078−1102

are grounded in experimentation for how functional groups, as individual species or through cooperative interactions, modulate controlled mineralization in animals.[11,31−34] The insights thus generated can further be applied to develop novel biomaterials for diverse applications.[35−40]

2. THE ORGANIC MATRIX IN BIOMINERALIZING ORGANISMS

Structural biology studies of biomineral-organic matrix associations show that biomineralization occurs in a physical compartment or otherwise "privileged space." A defining feature of this setting is an organic matrix of macromolecules in the form of gels and membranous substrates. The acidic composition, configuration, and activity of constituents in the organic matrix have long been implicated as critical in controlled biomineralization processes.[4,41,42]

The local biomineralization environment is generally characterized as intracellular or extracellular, although a continuum of arrangements is recognized.[11,43−45] As its name implies, intracellular mineralization occurs within cells and is typically controlled by the activities of cell membranes and specialized vesicles that regulate local chemical conditions such as pH and ion concentrations (Figure 3A). Mineral units that form within the vesicle are subsequently excreted to aggregate or transform into higher order structures.[44−47] Intracellular mineralization processes occur extensively in many single-celled organisms, e.g., calcification in coccolithophores,[48,49] silicification in diatoms,[50−53] or iron mineralization in magnetotactic bacteria.[54−56]

In contrast, extracellular mineralization takes place in regions outside, between, or connecting living cells (e.g., corals, mollusks, Figure 3B). In some settings, extracellular processes can also lead to passive mineralization whereby metabolic activities create conditions that favor spontaneous mineral precipitation. Examples are found in bacterial communities associated with some microbial mats, stromatolites, and eutrophic subsurface environments.[45,47,57,58]

At least three ongoing challenges impede our ability to adequately characterize the nature and activity of components in the organic matrix. First is the analytical challenge of extracting enough material from the mineral-organic composite for compositional analysis. A second, related difficulty is one of maintaining compositional integrity during the extraction processes. Changes in conformation and the loss of side chains that confer reactivity are particularly problematic.[59−64] Third, our current understanding of reactivity in the organic matrix is based upon studies that separated and characterized components according to solubility. Macromolecular solubility, while of practical importance, is a bulk property that reflects the general properties of the most durable components of the material after extraction and not necessarily the situation *in vivo*. It provides few details into the original matrix composition and structure, or regulation of biomineral formation. For example, the general term "acidic glycoprotein" is often the extent of identification that can confidently be made for *in vivo* macromolecules. Chitin, a major constituent of the organic matrix, is associated with the majority of identified proteins and polysaccharides at sites of mineralization (or partially identified components of these macromolecules).[59,65−69] However, the detailed nature of these associations could not be captured by traditional methods. Macromolecular characterization of the organic matrix and

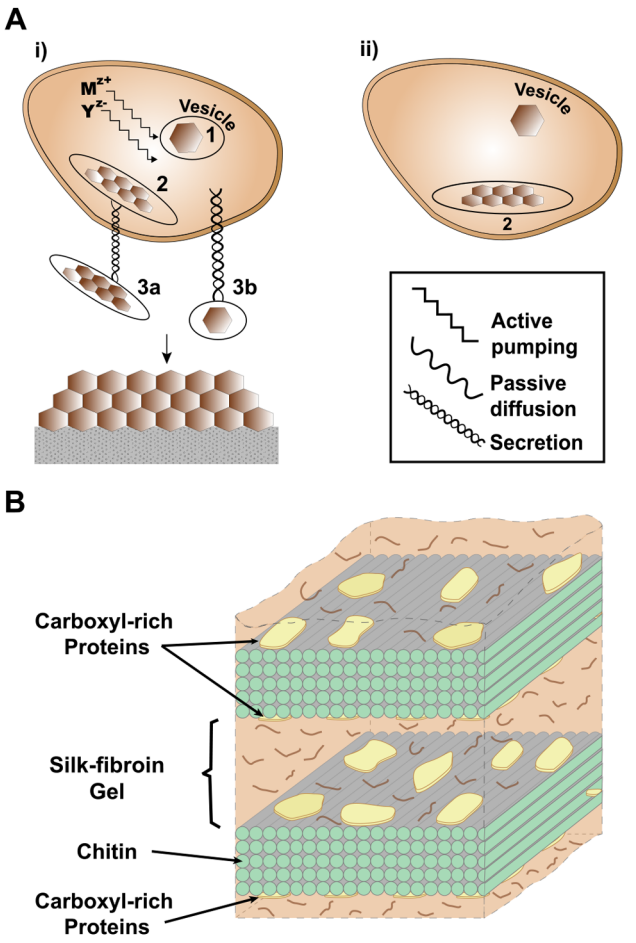

Figure 3. Schematic representation of biologically controlled mineralization. (A) Intracellular mineral nucleation from ions or amorphous precursors begins in a vesicle that is often rich in glycomaterials. The initial single crystals (1) or preformed units (2) are excreted onto a substrate (i, 3a, 3b) or remain in the vesicle (ii) (after Weiner and Dove, 2003).[45] (B) Extracellular mineral nucleation occurs in association with an organic matrix. In this example of the organic matrix in *A. serrata*, *β*-chitin sheets are associated with carboxyl-rich proteins and separated by a silk-fibroin gel that is thought to contain glycoproteins to produce nacre biominerals (after Levi-Kalisman et al., 2001).[43]

structure-property relationships continue to be major challenges.

2.1. Proteins. Owing to the nature of early extraction techniques, the biomineralization community traditionally focused on soluble proteins as the primary drivers in biogenic crystallization. Of particular interest is the abundance of aspartic and glutamic acid residues associated with glycoproteins.[16,29,41,70−72] The presence of acidic proteins within the organic matrix at sites of mineralization has given rise to a general consensus of a cause-effect relationship and motivated decades of research into the role of negatively charged amino acids on crystal nucleation and growth.[73−76] However, a closer look at macromolecular compositions suggests the relationships are more complex, with compounds often bound to acidic oligosaccharides or other polysaccharides (e.g., glycoproteins and proteoglycans).[16,65,66,77−79] Albeck and coauthors take a broader view by proposing a shared functionality whereby proteins control mineralization and polysaccharides "fine-tune" the process.[16] This lack of clarity about the

https://doi.org/10.1021/acs.biomac.2c01394
Biomacromolecules 2023, 24, 1078−1102

mechanistic roles of macromolecules and their functional groups raises the question of whether early postulations regarding relationships between organic matrix composition and mineralization are misleading. While providing insights, these conclusions from previous studies highlight an incomplete mechanistic understanding of the roles of macromolecules in biological crystallization.

2.2. Polysaccharides. Advances in structural biology and *in vitro* studies suggest polysaccharides may play more active roles in directing skeletal mineralization than previously recognized. Glycomaterials exhibit remarkable structural diversity that varies from simple monosaccharides and linear homopolymers to highly derivatized forms as well as extensively branched glycoproteins (Figure 4). Like the proteins of interest, polysaccharides associated with the organic matrices of Ophisthokonts at sites of calcification also exhibit acidic character.[28,78,81−83] Carboxylated polysaccharides are near-ubiquitous regardless of phylum, and an expanding body of literature is showing that sulfated and phosphorylated groups are also associated with these polysaccharides in many animals (Figure 5). The abundance of charged functional groups supports the idea that localized charge density, regardless of molecular class, regulates chemical activity during the onset of crystal formation. However, a closer look at the literature shows surprisingly little is known beyond general correlations. The compositions of polysaccharides in the organic matrix and their local associations with proteins, other polysaccharides, and lipids are not well-understood.

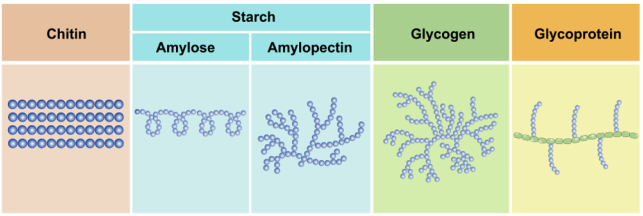

Figure 4. Simple illustrations of major polysaccharide groups show the structural diversity in the organization and general morphology of the polymer chains. Chitin and amylose, for example, are both linear homopolymers but have dissimilar monosaccharide composition, chain morphology, and organizations, while amylopectin and glycogen exhibit more complex branched structures. Not shown are the myriad variations that are possible in glycomaterials with differences in monosaccharide composition, bond position, configuration (α or β), or associated proteins (after Cornell, 2016).[80]

The vast structural variations that are possible in glycomaterials contribute to the challenge of associating polysaccharide and proteoglycans with functions in the biomineralization process. For example, monosaccharides can vary in oxidation state and functional group content, and the linkages between them can vary both in position and conformation, thus leading to exceptionally diverse macromolecule structures. It is therefore unsurprising that relationships between composition and skeletal features within or across animal groups are challenging to establish.

Polysaccharide complexity is also illustrated in algal examples. The calcifying marine algae, *E. huxleyi*, contains at least five polysaccharides comprising 14 different monosaccharides at sites of mineralization.[84] Of these, the composition of only one polysaccharide is known, and even its structural information remains incomplete. Alginate, found in brown algae, is composed of mannuronic acid (M) and guluronic acid (G) residues, where each monosaccharide features a charged carboxyl group; M-blocks are linear, while G-blocks are not. The nonlinearity of G-blocks produces an "egg-carton" shape with other alginate chains, creating pockets of carboxyl groups and enabling cross-linking with divalent cations (e.g., Ca^{2+}) to form a hydrogel.[85] Subtle modifications in monosaccharide sequence and M/G ratio generate changes in hydrogel properties, including stability and water content.

In other species (algal or otherwise), the composition and structure of a handful of polysaccharides have been identified, however, most studies simply detect polysaccharide presence

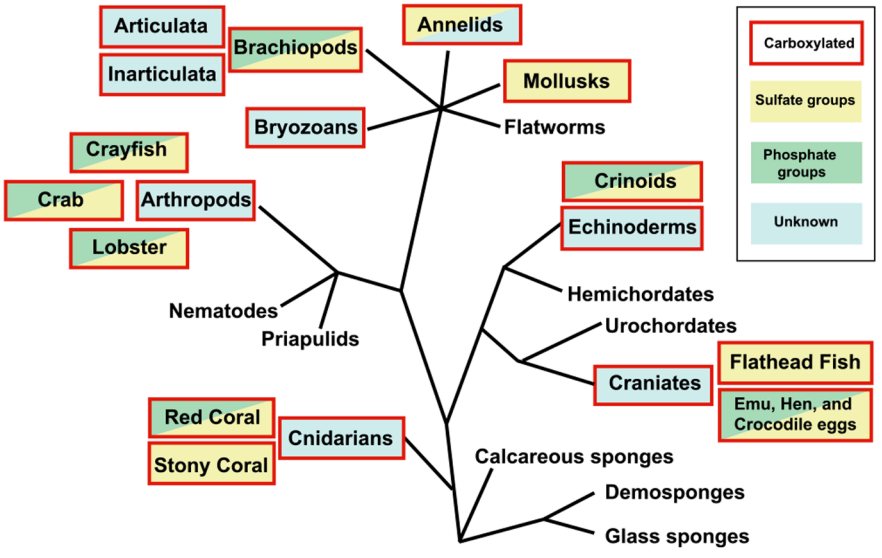

Figure 5. Reported distribution of carboxyl-, sulfate-, and/or phosphate-containing polysaccharides and glycoproteins associated with biominerals. Sulfate and phosphate groups are increasingly found to be associated with sites of mineralization alongside the carboxyl groups that traditionally are considered ubiquitous. "Unknown" indicates the macromolecules were identified as acidic glycoproteins or polysaccharides without detailed composition description (data from Table S1).

https://doi.org/10.1021/acs.biomac.2c01394
Biomacromolecules 2023, 24, 1078−1102

without further chemical information.[86] This ongoing difficulty of thorough separation and characterization for natural polysaccharides, compared to the historical emphasis on proteins, likely helps to explain the little attention given to polysaccharides in the biomineral community.

2.3. Focus on Chitin: Occurrence, Structure, and Solubility. Chitin is an abundant amido-polysaccharide (Figure 6A) found at sites of mineralization in marine animals.[81−83,87] This linear homopolymer is composed of glucosamine monosaccharides that are *N*-acetylated (Figure 6A). The D-2-acetamido-2-deoxyglucose repeat units are linked solely β-1,4. Thus, all substituents are in the equatorial plane. Three chitin polymorphs (α, β, and γ) are defined according to the orientation and associations of the individual chains into fibers (Figure 7). The most abundant polymorph is α-chitin (Figure 7A) and occurs as the predominant component in the exoskeletons of crab, lobster, shrimp, and krill, and the cuticles of insects.[87−89] Some fungal cell walls and eggshells also contain α-chitin.[88,90] The fibers can further organize into sheets via hydrogen bonding between individual chains and between sheets (Figure 8). This superior ability of α-chitin to form hydrogen bonds between sheets (due to their antiparallel orientation) confers remarkable strength as a structural polymer because the fibrils are tightly packed and bonded.[91,92] The efficiency of this arrangement may also assist crustaceans with osmotic controls that prevent the exoskeleton and hemolymph from both dehydration and swelling in water.[89,93] The less abundant β-chitin polymorph has parallel-oriented sheets (Figure 7B); it occurs, for example, in the pen and cuticle of squid.[89,92] γ-Chitin is a crystalline, structural mixture of the α and β forms (Figure 7C), found primarily in the larvae of insects such as beetles, cockroaches, dragonflies, and locusts.[92]

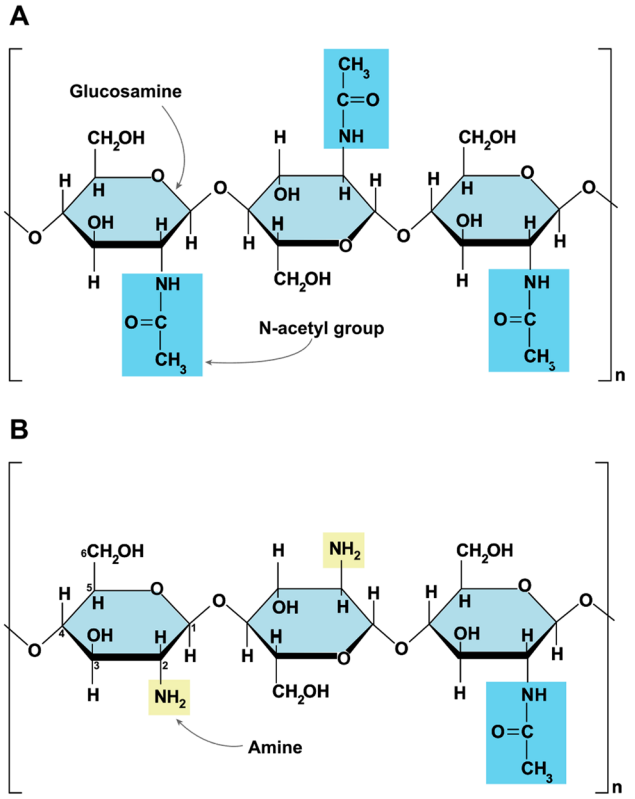

Figure 6. (A) Chitin is a linear polysaccharide composed of β-1,4 linked glucosamine monosaccharides that are *N*-acetylated at the C2 position (blue). (B) Chitosan is obtained by treating chitin with NaOH to yield amine groups (yellow) and a net positive charge on the molecule (see Section 3.2).

Figure 7. Three polymorphs of chitin are found that express variations in chain orientation. (A) α-Chitin with antiparallel chain organization; (B) β-chitin with parallel chains; and (C) the less-commonly observed γ-chitin is a structural mixture of α and β forms (after Roy et al., 2017).[91]

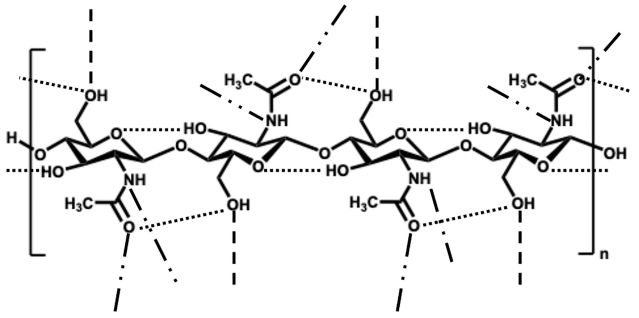

Figure 8. Hydrogen bonding network in α-chitin promotes organization into fibrils and sheets. Singular chains contain intramolecular hydrogen bonds (dotted lines) and chains are intermolecularly bonded to form sheets (dash dot dot dash). Additional intermolecular hydrogen bonding occurs between sheets (dash). β-Chitin exhibits similar hydrogen bonding but does not have intermolecular hydrogen bonding between sheets (after Chawla et al., 2015).[89]

Two examples show the complexity and intimate associations of polysaccharide and mineral. Chitin chains contained in the exoskeleton of the American lobster, *H. americanus*, are interwoven with acidic proteins and polysaccharides (Figure 9A).[66,95−97] The chains organize into sheets that comprise the endocuticle to become intercalated layers of polysaccharide and $CaCO_3$ as a biocomposite material.[96] Although details are yet to be established, similar interactions of silica with acetyl and hydroxyl groups of chitin chains are speculated to give rise to the SiO_2-reinforced spicules found in the marine glass sponge, *R. fibulata* (Figure 9B).[95] The resulting nanocomposite is composed of chitinous nanofibrils that are tightly enveloped by hydrated SiO_2 nanoparticles via hydrogen bonding.[95,98] These remarkable products of controlled mineralization reiterate the potential to create new materials if researchers can deconvolute macromolecule compositions and their contributions to biological crystallization. The

https://doi.org/10.1021/acs.biomac.2c01394
Biomacromolecules 2023, 24, 1078−1102

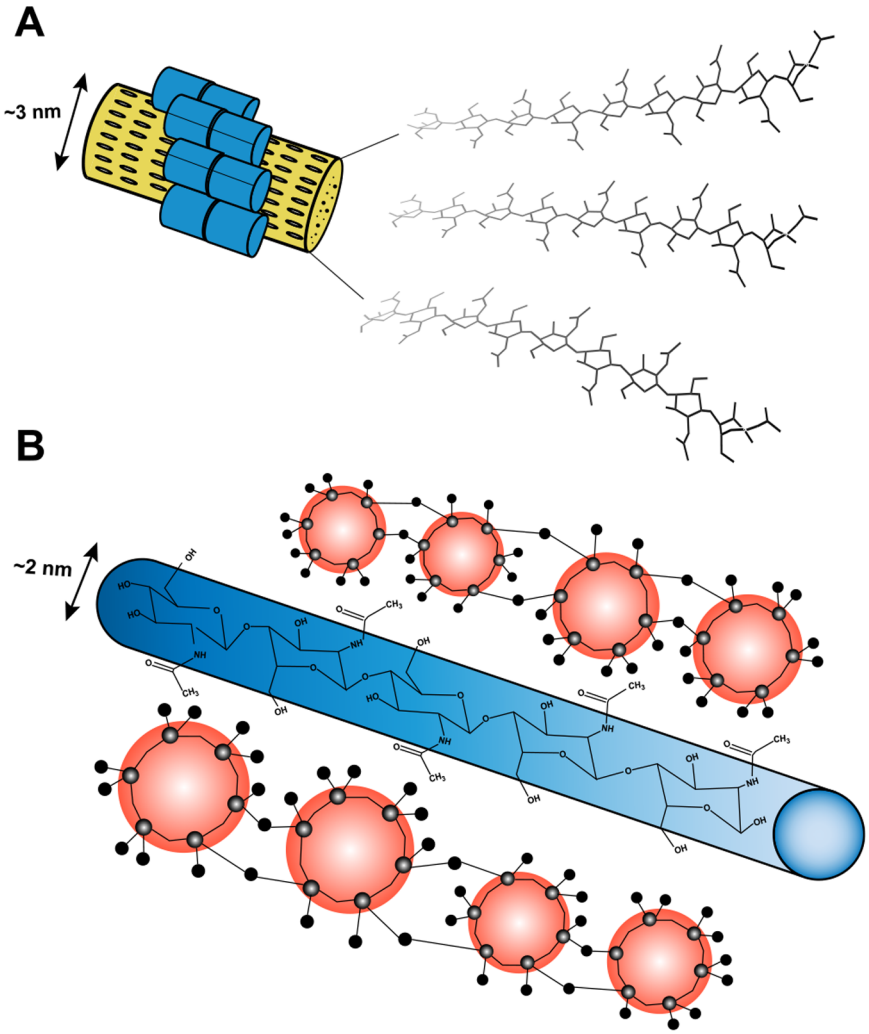

Figure 9. Schematic models for chitin organization in the organic matrices of two animals. (A) Endocuticle of American lobster (*H. americanus*) presents a hierarchy of chitin chain organization that shows a close association between chitin, calcite, and amorphous $CaCO_3$ (after Raabe et al., 2005).[96] Crystalline units of chitin chains (yellow) are wrapped with proteins (blue) to form nanofibrils. The nanofibrils further organize into fibers that make up a woven sheet containing $CaCO_3$-filled pores. (B) Model of silica-chitin interaction in the glass sponge (*R. fibulata*) shows hydrated silica (red) reinforces chitin nanofibrils (blue) via hydrogen bonding from −OH groups of silica to the −NAc and −OH groups of chitin. This close association gives way to a chamber-like structure that is proposed to assist with buoyancy control in *R. fibulata* (after Ehrlich, 2010).[95]

possibility of underlying systematics also suggests that relationships between macromolecule composition and structure and chemical activity in the organic matrix are an important frontier of biological science.

Only a few investigators have explored chitin properties and structure-property relationships related to mineral crystallization, and the potential to innovate new chitin-based materials.[95,99−102] A major limitation in studies of chitin is its low solubility. Although the repeat unit is polar (e.g., Figure 6A), the extensive hydrogen bonded network of the chitin chains and sheets (Figure 8) prevents dissolution in aqueous media. Chitin is also insoluble in all single organic solvents. Its high crystallinity prevents thermal processing since it lacks glass (T_g) or melting (T_m) transition temperatures. Chitin degrades before reaching either (theoretical) glass or melting temperatures. These refractory properties have made chitin a challenging material to investigate or process for practical applications.

3. PREVIOUS STUDIES OF CHITIN AND CHITOSAN INFLUENCE UPON $CACO_3$ CRYSTALLIZATION

Numerous studies have explored the effects of organic components extracted sites of biomineralization in animals on $CaCO_3$ mineralization. Most have been qualitative and observational descriptions of the formed $CaCO_3$ polymorphs and morphologies with little quantitative control or characterization of the corresponding solution compositions. For example, few studies elucidated (or held constant) supersaturation during an experiment. This is critical to quantifying the chemical driving force for precipitation and thus to determining kinetic or thermodynamic properties of crystallization. While these reports provide insights that may aid design of future studies, they reinforce the argument that a consistent picture of mineralization in the presence of chitin-based compounds has not emerged.

3.1. Chitin. Broadly speaking, there have been three categories of studies involving chitin. In the first, authors studied nucleation of $CaCO_3$ onto chitin itself, in various

https://doi.org/10.1021/acs.biomac.2c01394
Biomacromolecules 2023, 24, 1078−1102

Table 1. Summary of Selected Studies of $CaCO_3$ Nucleation onto or in the Presence of Chitin (Native, Partially Decomposed, or Derivatized)

Substrate	$CaCO_3$ Polymorph and Morphology	Method and Notes	Reference
Chitin	Calcite	Quantitative, constant composition method, pH 8.5, γ = 27 mJ m^{-2}	Manoli et al. (1997)[103]
Chitin from *A. Psittacus* (barnacle) deproteinized by formic acid	Calcite	Qualitative, ammonium carbonate method, deproteinization also caused some deacetylation of chitin	Fernandez et al. (2015)[104]
Chitin from *A. Psittacus* (barnacle) deproteinized by Dowex	Calcite with curved faces and vaterite aggregates		
Chitin (low yatalase conc.)[a]	Calcite, polygonal, lattice distortion	Qualitative, ammonium carbonate method	Kintsu et al. (2017)[105]
Chitin (high yatalase conc.)[a]	Rounded calcite, increased lattice distortion		
Chitin gel	Rhombohedral calcite	Qualitative, ammonium carbonate method	Kintsu et al. (2017, 2021)[105,107] Perez-Huerta et al. (2019)[106]
Chitin nanofibers	Calcite with altered rhombohedral		
Chitin gel (low yatalase conc.)[a]	Calcite, rough and altered rhombohedral	Qualitative, ammonium carbonate method, suggest chitin degradation causes slight defects which increase mechanical strength of shell	Perez-Huerta et al. (2019),[108] Kintsu et al. (2021)[107]
Chitin gel (high yatalase conc.)[a]	Calcite, rounded rhombohedral, lattice distortion		
Phosphorylated chitin	Calcite and vaterite	Qualitative, electro-crystallization method, inhibition seen, no replicates reported	Butto et al. (2018)[109]

[a]Chitin treated with yatalase (chitinolytic enzyme).

Table 2. Selected Studies of $CaCO_3$ Nucleation on or within Chitinous Organic Matrices (OMs)

Organic Matrix/Substrate	$CaCO_3$ Polymorph and Morphology	Method and Notes	Reference
OM of *A. calycularis* (coral)	Agglomerates and modified calcite	Qualitative, ammonium carbonate method	Reggi et al. (2016)[61]
OM of *B. europaea* (coral)	Agglomerates and modified calcite		
OM *of S. pistillata* (coral)	Spherical crystals		
Lipid OM of *A. calycularis*	Calcite and vaterite	Qualitative, ammonium carbonate method, extraction likely removed some lipids/macromolecules	
Lipid OM of *B. europaea*	Calcite and vaterite		
Lipid OM *of S. pistillata*	Calcite		
OM of *L. foecundum* (coralline algae)	Mg-calcite: aragonite 30:70	Qualitative, gas diffusion method, OM contains glycoproteins	Rahman et al. (2019)[64]
Untreated nacre (unspecified species)	Tightly packed needle aragonite	Qualitative, direct mixing, treated nacre suggests residual protein effect, untreated has (001)-orientation	Chen et al. (2016)[110]
HCl treated nacre (unspecified species)	Pyramid shaped $CaCO_3$		
NaOH treated nacre (unspecified species)	Nonuniform $CaCO_3$ coating		
OM of *P. fucata* (bivalve) with chitinolytic enzymes inhibited	Abnormal shell and OM structure, thicker chitin	Qualitative, *in vivo*, enzymes inhibited by injecting organism with allosamidin	Kintsu et al. (2017, 2021)[105,107]
Insoluble OM from *A. Psittacus* (barnacle)	Calcite with (001) orientation	Qualitative, direct mixing, insoluble organic matrix contains chitin and sulfated proteoglycans	Rodriguez-Navarro et al. (2021)[111]
Milled scallop shells	Calcite, layered	Qualitative, direct mixing	Wakayama (2020)[112]
Internal shell of *A. californicus* (slug)	Altered/rounded calcite	Qualitative, ammonium carbonate method, at increased [$CaCl_2$], vaterite also nucleates	Montroni et al. (2021)[113]
Soluble OM from *A. Psittacus* (barnacle) with deproteinized chitin from insoluble OM	Vaterite that transformed to rounded calcite, then rhombohedral	Qualitative, ammonium carbonate method, deproteinization also caused some deacetylation of chitin	Fernandez et al. (2015)[104]

forms, or chitin that had been partially degraded. As presented in Table 1, calcite is the dominant polymorph to crystallize in the presence of any form of chitin (substrate,[103,104] gel,[105−107] or nanofiber[105−107]). In studies where chitin was treated with yatalase, a chitinolytic enzyme, a change in morphology was observed from rhombohedral to roughened or rounded rhombohedra. The authors suggested that partial degradation of chitin increases the mechanical strength of biomineral features (e.g., an organism's shell) through small crystal defects and lattice distortions.[105−107]

To our knowledge, only one investigation measured the kinetics of $CaCO_3$ nucleation onto chitin. Using the constant composition method (quantitative) of measuring the rate of $CaCO_3$ precipitation, chitin was added to a supersaturated solution of calcium carbonate into which base and acid were titrated to maintain a constant pH. The resulting polymorph was calcite as determined by scanning electron microscopy (SEM). By evaluating rate data collected at different supersaturations, the authors found that chitin dramatically lowered the barrier to calcite nucleation compared to that of bulk solution.[103]

3.1.1. Organic Matrices. In a second category of studies, the chitinous organic matrices of organisms were extracted and authors report the $CaCO_3$ polymorphs that nucleated in the presence of these materials (Table 2). For example, Reggi et al. (2016) isolated the intraskeletal organic matrix from the extracellular matrix of three corals from diverse ecologies and that produce different types of reef structures (*A. calycularis*, *B. europaea*, *S. pistallata*).[61] In the presence of the whole intraskeletal organic matrix that contained soluble and

https://doi.org/10.1021/acs.biomac.2c01394
Biomacromolecules 2023, 24, 1078−1102

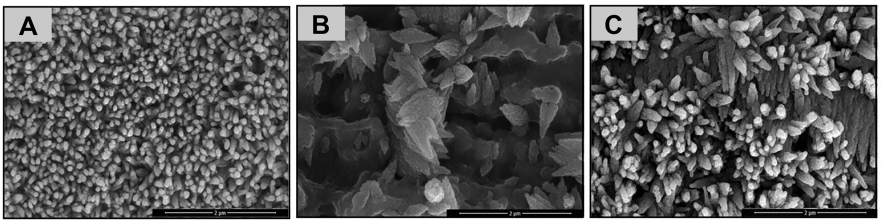

Figure 10. SEM images of $CaCO_3$ nucleation on (A) untreated nacre (B) acid treated, and (C) alkaline treated. Textures show the contrasting organizations between the "raw" organic matrix (A) and those with removed macromolecules (B, C). Scale bar = 2 μm. Reproduced from *Powder Technology*. Copyright 2016, with permission from Elsevier.[110]

insoluble organic fractions, calcite precipitated in the form of agglomerates and modified spherical crystals in contrast to the aragonite polymorph that is mineralized by coral-producing organisms in modern oceans. Recognizing that macromolecules in the organic matrix likely have mutual interactions, the lipid portion of the organic matrix was extracted for an additional nucleation study.[61] Depending upon the coral species, the lipid component produced calcite with varying amounts of vaterite. Overall, the number and size of particles were smaller in the presence of the lipid portion compared to the whole organic matrix. This observation led to the suggestion that template and nucleator act together to encourage nucleation and to promote the nucleation of more stable polymorphs.[61] However, the extraction method for the lipids employed harsh conditions which likely degraded an undetermined portion of the macromolecules present. Thus, it is possible that some components affecting nucleation were altered or missing.

A number of observational studies support the premise that the organic matrix influences mineralization by modifying $CaCO_3$ morphology and polymorph. For example, Chen et al. (2016) investigated $CaCO_3$ mineralized onto an unspecified type of fresh nacre (organic-inorganic composite of the inner shell produced by some mollusks) that was subjected to two treatments: acidic (HCl, demineralizes and alters some macromolecules) and alkaline (NaOH, removes some macromolecules), and the results were compared to those obtained on an untreated control sample.[110] The crystallites that nucleated onto the untreated nacre (Figure 10A) showed the greatest coalignment and similar morphology compared to those formed on nacre where a portion of the organic matrix was removed by chemical treatment (Figure 10BC).[110]

Some studies in this group also treated isolated or otherwise-sourced chitin with the extracted soluble organic matrices (or portions thereof) of organisms (Table S2). All studies in this category illustrate the diverse and complex effects of macromolecules in the organic matrix but share a lack of characterization and therefore are hard to interpret in the context of building a broader mechanistic picture.

3.1.2. Isolated Chitin as a Substrate for Macromolecules. A third group of studies investigated $CaCO_3$ formation in the presence of chitin isolated from marine animals and treated with only one type of (partially) characterized macromolecule (Table 3). While the simpler experimental design cannot sufficiently mimic *in vivo* environments, the use of materials without impurities and/or unknowns permits better control of mineralization experiments, generating findings that are more readily interpreted.

For example, using a phosphorylated, calcification-associated peptide (CAP-1) from the exoskeleton of a crayfish (*P. clarkia*), Sugawara et al. (2006) compared $CaCO_3$ crystallization onto chitin in the presence of CAP-1 versus its nonphosphorylated analog (rCAP-1).[114] Rhombohedral calcite nucleated onto chitin alone (control). In the presence of CAP-1, a thin film of calcite with a (001)-preferred orientation formed, while in the presence of rCAP-1, oriented calcite nucleated, but not in the form of a thin film. The authors further modified the peptides to investigate only the acidic C-terminus (shortened peptide chain) of both CAP-1 and rCAP-1. The phosphorylated material formed $CaCO_3$ crystals with a hemispherical morphology in contrast to the nonphosphorylated material which nucleated peanut-shaped crystals (polymorphs unspecified). Neither exhibited a preferred crystal orientation. The authors suggested that the order and length of the acidic residues associated with the peptide stabilize binding with chitin to promote oriented crystal growth, while the phosphate residue helps to stabilize amorphous polymorphs.[114] This loss of orientation could also indicate that the modification changed the arrangement of functional groups on the substrates.[126] Kumagai et al. (2012) similarly observed the occurrence of (001)-oriented, platelike calcite on chitin in the presence of modified rCAP-1 with repeating acidic residues, in contrast to no orientation in the presence of the shorter repeating acidic residues alone. These authors also postulated that chain order and length contributed to stronger peptide binding to chitin, resulting in the observed differences in morphology.[115] Previously, CAP-1 was considered a $CaCO_3$ nucleation inhibitor when studied in solution without chitin.[127]

Others investigated $CaCO_3$ crystallization onto composites of poly(acrylic acid) (PAA) and chitin. Owing to the carboxyl moieties present on each repeat unit, PAA is a valuable proxy for exploring the influence of carboxyl-rich proteins on mineralization and has been extensively studied by Laurie Gower and others.[128,129] As with CAP-1, PAA is considered an inhibitor in aqueous suspensions, but behaves differently in the presence of a template.[130,131] Munro and McGrath (2012) showed that, in the presence of chitin, PAA induced aragonite formation in contrast to the calcite formed in the presence of chitin alone.[123] Later, Munro, Green, and McGrath (2013) introduced chitosan oligomers to the system of chitin and PAA and also observed aragonite formation.[124] Intriguingly, most of the $CaCO_3$ crystals formed at the chitin-oligomer interface (Figure 11). Both studies suggest the possibility of cooperative interactions between the functional groups of chitin and functionalized macromolecules.

One group investigated how the interactions between PAA and the hydroxyl (−OH) and *N*-acetyl (−NHAc) functional groups of chitin affect $CaCO_3$ nucleation. Nucleation in the presence of PAA and chitin produced thin calcite films (control). In a system containing PAA and a chitin derivative with blocked −OH groups, little to no difference from the control was seen. In contrast, no nucleation was observed in

https://doi.org/10.1021/acs.biomac.2c01394
Biomacromolecules 2023, 24, 1078−1102

Table 3. Selected Studies of $CaCO_3$ Nucleation onto Chitin in the Presence of Identified Macromolecules

Substrate (with chitin)	$CaCO_3$ Polymorph and Morphology	Method and Notes	Reference
CAP-1[a]	Calcite, thin films	Qualitative, direct mixing, crystals overall smaller when phosphorine residue present, suggest long peptide chains assist in film formation	Sugawara et al. (2006)[114]
rCAP-1[b]	Blocky calcite, oriented		
pSSED6[c]	Half-dome, polymorph unspecified, no orientation		
S2ED6[d]	Peanut-shaped, polymorph unspecified, no orientation		
rCAP-1-CD[e]	Plate-like tripodal calcite, (001) orientation	Qualitative, gas diffusion method, peptide contains repeating acidic residues at c-terminus	Kumagai et al. (2012)[115]
rCAP-1-CT[f]	Plate-like tripodal calcite, no orientation		
CD[g]	Plate-like tripodal calcite, no orientation		
CT[h]	Plate-like tripodal calcite, no orientation		
Pif 97, Pif 80, N16[i]	Aragonite and vaterite, (001) orientation	Qualitative, gas diffusion method, Pif proteins contain cysteine residues	Suzuki et al. (2009)[116]
Artificial protein containing chitin- and calcite-binding domains	Calcite and vaterite	Qualitative, enzyme (urease)-induced carbonate precipitation, protein alone nucleated cauliflower shaped calcite	Nawarathna et al. (2021)[117]
PLL4[j] and chitin monosaccharides	Calcite, small and numerous	Qualitative, ammonium carbonate method, artificial seawater	Ogawa et al. (2021)[118]
PLL4 and chitin oligomers	Calcite, large and few		
Poly (Asp)	Aragonite majority with calcite and vaterite	Qualitative, ammonium carbonate method	Levi et al. (1998)[119]
Poly (Glu)	Calcite majority with some aragonite and vaterite		
Poly (Asp-Leu)	Aragonite		
Silk fibroin from *B. mori* (moth)	Vaterite	Qualitative, direct mixing	Falini et al. (1996)[120]
Poly (Asp) in chitin-silk fibroin complex	Calcite majority with some	Qualitative, ammonium carbonate method	Levi et al. (1998)[119]
Poly (Glu) in chitin-silk fibroin complex	Vaterite		
PAA[k]	Calcite, thin films	Qualitative, gas diffusion method, repetition of polymer and $CaCO_3$ coatings	Kato et al. (2000)[121]
PAA (low MW)	Calcite, thin films	Qualitative, gas diffusion method, % calcite increased with [PAA], −OH groups inhibited by acetylation	Hosoda and Kato (2001)[122]
PAA (high MW)	Calcite and vaterite, thin films		
Chitin with −OH groups inhibited and PAA	Thin film $CaCO_3$, polymorph unspecified		
PAA with 10 wt % chitosan oligomers	Aragonite	Qualitative, gas diffusion and direct mixing combo method, reacetylated chitosan, edge between chitin and oligomers preferentially mineralized	Munro and McGrath (2012)[123] Munro, Green, and McGrath (2013)[124]
PAA/Mg^{2+}	Aragonite	Qualitative, gas diffusion method, synthetic nacre, nucleation centers at areas with PAA	Mao et al. (2016)[125]

[a]Calcification-associated peptide from *P. clarkia* (crayfish). [b]Recumbant peptide of CAP-1, no phosphorine residue. [c]Acidic C-terminus of CAP-1. [d]Acidic C-terminus of rCAP-1. [e]Altered rCAP-1 with 2 acidic repeat sequences at C-terminus. [f]Altered rCAP-1 with 3 acidic repeat sequences at C-terminus. [g]Acidic oligopeptide with 2 repeat sequences. [h]Acidic oligopeptide with 3 repeat sequences. [i]Isolated matrix proteins of *P. fucata* (mollusk). [j]Lectins from *P. penguin* (mollusk). [k]Poly(acrylic acid) .

https://doi.org/10.1021/acs.biomac.2c01394
Biomacromolecules 2023, 24, 1078−1102

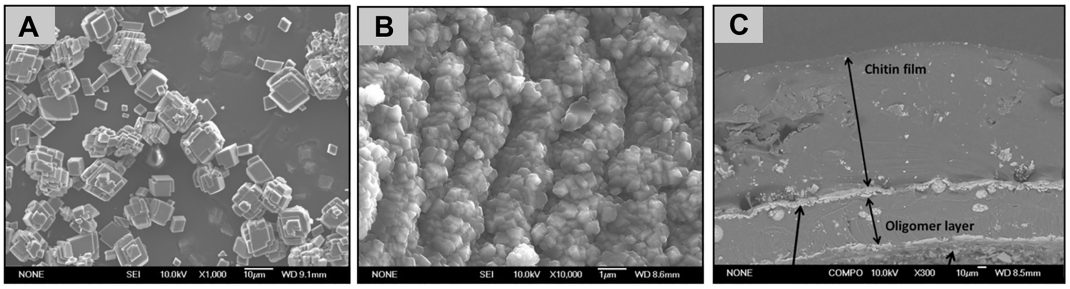

Figure 11. SEM images show $CaCO_3$/ chitin composite materials that form using a chitin template soaked in mineralizing solutions in the (A) absence or (B, C) presence of PAA. Chitin oligomers were added to the solution in (C) to produce mineralization at the interface of the layers, indicated by arrows. Scale bar = 10 μm (A, C) and 1 μm (B). Used with permission of the Royal Society of Chemistry, from *Chemical Communications*, (A,B);[123] (C);[124] permission conveyed through Copyright Clearance Center, Inc.

the presence of PAA and a chitin derivative with both hydroxyl and amine groups protected.[121,122] Recent studies suggest polymer-induced liquid precursors (PILPs) may play an important, albeit indirect, role in promoting ion infiltration to sites of (calcium phosphate) mineralization, but nucleation of a solid phase is promoted by charged residues on a scaffold or by complexation of PILP molecules with the scaffold, rather than by PILP alone.[132,133] The studies discussed here and shown in Table 3, using chitin as a substrate, demonstrate the potential for an improved understanding of specific template-nucleator interactions.

3.2. Chitosan. Chitosan is a general term for partially deacetylated chitin, i.e., chitin lacking a fraction of its original *N*-acetyl (CH_3CO, Ac) groups (Figure 6B). Natural chitosans exist, for example in many fungal cell walls.[134] Commercial chitosan, however, is typically prepared by chemical or enzymatic hydrolysis of marine chitin (primarily shrimp cuticle).

3.2.1. Background to Chitosan Properties. Descriptions of chitosan compositions are based upon the partial deacetylation of chitin, commonly expressed as the fraction that remains acetylated (F_A) or degree of acetyl substitution (DS(Ac)) (e.g., Figure 6B). The extent of deacetylation of amides to amines can be controlled by adjusting the reaction stoichiometry and the synthesis conditions including temperature, [NaOH], and duration of alkaline hydrolysis.[135,136] At sufficiently low DS(Ac) ($\leq$0.6; therefore DS(amine) $\geq$ 0.4), the molecule becomes sufficiently ionic to increase the bulk solubility of chitosan. This enhanced solubility vastly expands synthetic and processing possibilities, and thereby, applications.[89,135,137−139] During alkaline hydrolysis, there is some reduction in the degree of polymerization (DP) via alkaline peeling, but products of significant DP (up to several thousand repeat units) can be isolated.[89]

The solubility of chitosan has a complex dependence on pH that is determined by an interplay of DS(Ac), DP, and polymer morphology. To illustrate, Figure 12 shows that chitosan is soluble in aqueous solutions of pH < 6 regardless of DS(Ac) and molecular weight (proportional to DP). Chitosan pK_a has been reported to be approximately 6.0.[140] However, in mildly acidic to basic solutions, chitosan solubility is dependent upon DS(Ac) (e.g., in Figure 12 compare samples CS4 and HCS2) and molecular weight (e.g., CS4 and CS0). Materials with DS(Ac) of 0.4 to 0.6 show the broadest pH range of high solubility.[89,141−143] Polymer morphology is also important such that a more random distribution of acetylated and deacetylated monosaccharides affords higher solubility than

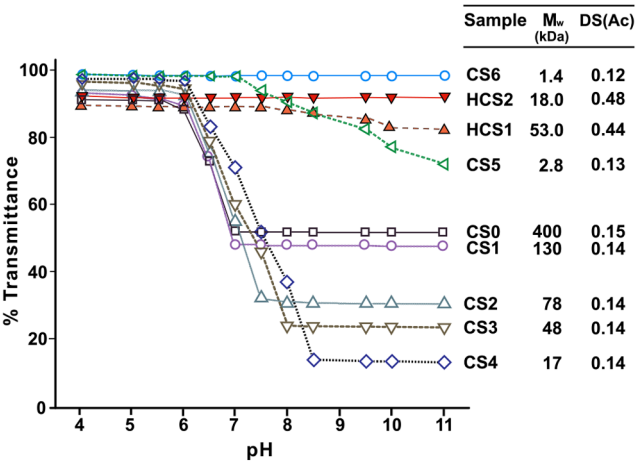

Figure 12. Solubility of chitosan vs pH for materials with different DS(Ac) and molecular weights. Lower % transmittance indicates greater turbidity due to polysaccharide precipitation and thus correlates with lower solubility. It can be seen that chitosan of DS(Ac) 0.40−0.60 gives the broadest range of solubility, but any chitosan with DS(Ac) < 1 becomes soluble in acidic conditions. Lower molecular weight also enhances chitosan solubility. Chitin has a DS(Ac) of 1.00 and would be represented on this plot as a line at very low transmittance (after Qin et al., 2006).[143]

blocky polymers, where monosaccharide self-association reduces solubility.[142]

3.2.2. $CaCO_3$ Nucleation in the Presence of Chitosan Alone. Investigations of $CaCO_3$ nucleation in the presence of chitosan alone as a substrate, solution, or gel are given in Table 4. As in the presence of chitin, rhombohedral calcite was the primary polymorph that formed, but unlike with chitin, more polymorphic and morphologic variability was reported for $CaCO_3$ nucleated onto different physical states of chitosan. For example, Xiao et al. (2008) observed rhombohedral calcite precipitated in a chitosan solution, but vaterite plates were produced when chitosan was present in gel form.[144] The $CaCO_3$ polymorph and morphology that nucleates also appears to be sensitive to experimental method. Using cryogels, Vasiliu et al. (2021) used three experimental methods to observe $CaCO_3$ nucleation and growth (alternate dipping, hydrolysis, ammonium carbonate) and noted three different results.[145] However, it is important to recognize that the DS(Ac) of chitosan used in all of these studies may have varied. This important characteristic, with great influence on

https://doi.org/10.1021/acs.biomac.2c01394
Biomacromolecules 2023, 24, 1078−1102

Table 4. Selected Studies of $CaCO_3$ Nucleation onto Chitosan Alone

Substrate	$CaCO_3$ Polymorph and Morphology	Method and Notes	Reference
Chitosan	Rhombohedral calcite	Quantitative, pH 10, γ = 51 mJ m^{-2}	Giuffre et al. (2013)[146]
Chitosan	Rhombohedral calcite	Control experiments from Table 6	–
Chitosan	Aragonite and calcite mixture	Qualitative, direct mixing	Wakayama (2020)[112]
Chitosan in solution	Calcite	Qualitative, direct mixing, authors suggest chitosan self-association in solution and stereochemical matching in gel are responsible for polymorph	Xiao et al. (2008)[144]
Chitosan gel	Hexagonal vaterite plates		
Chitosan cryogel	Rhombohedral calcite and spherical vaterite	Qualitative, alternate dipping method	Vasiliu et al. (2021)[145]
Chitosan cryogel	Calcite, rhombohedral, and aggregates	Qualitative, hydrolysis of dimethyl- or diethyl-carbonate	
Chitosan cryogel	Vaterite that transforms into rhombohedral calcite	Qualitative, ammonium carbonate method, uniform layers formed	

chitosan properties, is not always measured or characterized for nucleation studies (Table S3).

In a quantitative investigation, Giuffre et al. (2013) systematically studied how chitosan and other polysaccharides influence $CaCO_3$ nucleation.[146] By varying functionality and net charge density, they showed the rate of calcite nucleation is polysaccharide-specific. Fitting their experimental measurements to classical nucleation rate theory (see Sections 5.1, 5.2), they found the energy barrier to calcite nucleation was proportional to the net charge of the corresponding monosaccharide unit. They found chitosan presents the lowest energy barrier to nucleation whereas heparin (carboxyl and sulfate groups) and alginate (carboxyl-dense) substrates have the highest barriers.[146] Studies of calcite nucleation onto functionalized self-assembled monolayers report the same trend.[126] These findings support the hypothesis that the energy barrier correlates with net polysaccharide charge, across multiple types of functional groups.

3.2.3. Chitosan Derivatives. Tailored functionalization of chitosan is a feasible way to overcome the insolubility of chitin and the pH-dependent solubility of chitosan (most chitosans are not aqueous-soluble at neutral or higher pH). This capability has motivated diverse investigations of how to synthesize derivatives for new and existing applications, but to our knowledge relatively few studies were directed at understanding the influence of their properties upon $CaCO_3$ formation (Table 5). Several of these studies explored the effects of carboxymethyl chitosan (CMCS)—chitosan functionalized with carboxyl groups to varying degrees (DS(CM))—on the precipitation of $CaCO_3$ for applications as a bioadditive to paper[147] or as a scale inhibitor in oil-brines.[148,149] It is likely that a substantial motivation for these studies is the high solubility of CMCS in pure water, in contrast to most chitosans that require an acetic acid cosolvent. The findings generally support the notion that an increased concentration of CMCS in the nucleating system (regardless of DS(CM)) leads to less stable polymorphs, often with unusual morphologies and decreased particle size.[147−152] Interpretations across (and sometimes within) the CMCS studies are impeded by the wide range of DS(CM) that spanned 0.2 to 1.6. Owing to this variability in composition and the inconsistent protocols, these studies provide little quantitative insight into how the composition of CMCS influences $CaCO_3$ nucleation.

3.2.4. Chitosan as a Substrate for Studies of Other Macromolecules. Using chitosan as a model organic matrix, a number of qualitative studies introduced functionalized macromolecules to investigate their potential role in $CaCO_3$ nucleation using a variety of experimental techniques and solution compositions (Table 6). Many researchers investigated the role of carboxylated macromolecules on $CaCO_3$ mineralization by employing chitosan as a substrate in studies of PAA (Table S4). Using a variety of observational techniques, many types of solution compositions were studied. All of the common crystalline polymorphs were formed, including amorphous calcium carbonate, in variable ratios (e.g., Table S4). Numerous morphologies were reported including rhombohedral, spherical, columnar, and films; no clear trends were observed.

The diversity in film morphologies well-illustrates the breadth of PAA results. For example, Kato et al. (1998, 2000) used a gas diffusion method and observed the formation of thin film calcite where vertical growth was further suppressed as the concentration of PAA increased.[121,165] Li et al. (2021) also observed the formation of calcite thin films using a direct mixing method and noted that the films began as disks at sites of high concentration of PAA/carboxyl groups.[173] Contrarily, when $CaCO_3$ films were formed onto PAA by Wada et al. (2004) or Suzuki et al. (2016) (both using the ammonium carbonate method), they were comprised of aragonite and vaterite.[168,174] Wada et al. (2004) observed $CaCO_3$ crystallites with a (001) preferred orientation,[174] while Suzuki et al. (2016) observed *c*-axis inhibition.[168]

Others investigated the extent of $CaCO_3$ mineralization on chitosan using variable PAA concentrations in efforts to determine structure-property relationships. Payne et al. (2007) observed that $CaCO_3$ growth was promoted until reaching a threshold PAA concentration.[175] Above this level, crystal growth was inhibited as evidenced by fewer and more distorted crystals. However, like most other studies, their crystallization methodology presented a variable and uncontrolled chemical driving force (supersaturation) over the course of the experiments. Some authors reported that low concentrations of PAA have a small inhibiting effect on $CaCO_3$ formation that increases to full inhibition with increasing concentration.[71,110,121]

Also common in this group are investigations of polypeptides including poly(aspartic acid),[161−163] poly(glutamic acid),[164,165] and rCAP-1.[115] These peptides affected $CaCO_3$ morphology in similar fashion and produced disk-like, thin films. However, peptide concentrations and experimental conditions correlated with changes in polymorph distribution.

Few studies explored the effect of charged polysaccharides in the presence of chitosan upon $CaCO_3$ nucleation, and to our

https://doi.org/10.1021/acs.biomac.2c01394
Biomacromolecules 2023, 24, 1078−1102

Table 5. Studies of $CaCO_3$ Nucleation onto Chitosan Derivatives

Substrate	$CaCO_3$ Polymorph and Morphology	Method and Notes	Reference
CMCS[a], 1% DS(CM) = 0.23	Mixture of calcite and vaterite with minimal aragonite	Qualitative, scale inhibitor test, crystal size decreased as [CMCS] increased	Bolivar et al. (2021)[149]
CMCS, 1% DS(CM) = 0.40	Mixture of calcite and vaaterite with minimal aragonite		
CMCS, 2% DS(CM) = 0.23	Aragonite and calcite		
CMCS, 2% DS(CM) = 0.40	Majority vaterite		
CMCS DS(CM) = 0.45−0.50	Deformed calcite and vaterite	Qualitative, scale inhibitor test, above threshold [CMCS], no nucleation was observed	Macedo et al. (2019)[148]
CMCS DS(CM) = 0.91	Aggregates of spherical nanocrystals, vaterite and calcite	Qualitative, ammonium carbonate method, % calcite smaller than solution alone but increased as [CMCS] increased	Yang et al. (2010)[152]
CMCS DS(CM) = 0.98	Calcite and aragonite	Qualitative, direct mixing, % aragonite and crystal size decreased as [CMCS] increased	Fortuna et al. (2021)[147]
CMCS DS(CM) = 1.57	Calcite, rhombohedral, irregular rhombohedral, spherical, and peanut shaped	Qualitative, direct mixing, particle size decreased as [CMCS] increased	Liang et al. (2004)[151]
CMCS, low conc. DS(CM) = 1.57	Linear aggregates	Qualitative, gas diffusion method, at low concentrations, calcite increases as [CMCS] increases (up to a threshold past which no nucleation is observed)	Liang et al. (2004)[150]
CMCS, high conc. DS(CM) = 1.57	Petunia shaped mixture of calcite and vaterite, rhombohedral calcite		
HMB-CMCS[b] 1:4, low conc.	Rhombohedral calcite and spherical vaterite	Qualitative, direct mixing, higher conc. nucleated smaller particles	Huang et al. (2007)[153]
HMB-CMCS 1:4, high conc.	Peanut shaped calcite		
O-(hydroxy isopropyl) chitosan	Passivated rhombohedral calcite	Qualitative, direct mixing, coupled with computational molecular dynamics study of polymer-104 face interactions	Yang et al. (2009)[154]
HTCC[c]	$CaCO_3$, all polymorphs, various morphologies (rhombohedral, disk, and rod)	Qualitative, ammonium carbonate method, HTCC distorts crystal lattice	Wang et al. (2016)[155]
CTS-MA-SSS-AM[d] 1.8:1:3:.072	$CaCO_3$, polymorph unspecified, 96% inhibition compared to solution alone	Qualitative, scale inhibitor test	Guo et al. (2012)[156]
Chitosan biguanidine hydrochloride	Small crystals, polymorph unspecified	Qualitative, scale inhibition, delayed induction time	Maher et al. (2020)[157]
Histidine grafted chitosan	Spherical vaterite/calcite	Qualitative, direct mixing, increased [histidine grafted chitosan] gave more vaterite, increased time gave less vaterite	Chen et al. (2017)[158]
Polyacrylamide grafted chitosan (low MW)	Spherical crystals	Qualitative, ammonium carbonate method, some $CaSO_4$ also present due to cross-linker releasing SO_4^{2-}	Niera-Carrillo et al. (2005)[159]
Poly(vinyl sulfonic acid) grafted chitosan	All polymorphs, various morphologies (spherical, disk, prismatic, needle)	Qualitative, ammonium carbonate method, $CaSO_4$ also present due to cross-linker releasing SO_4^{2-}	Niera-Carrillo et al. (2011)[160]

[a]Carboxymethyl chitosan. [b]2-Hydroxyl-3-butoxylpropyl-hydroxymethyl chitosan. [c]*N*-[(2-hydroxyl)-propyl-3-trimethylammonium] chitosan chlorite. [d]Chitosan-maleic anhydride-styrene sulfonic sodium-acrylic amide.

https://doi.org/10.1021/acs.biomac.2c01394
Biomacromolecules 2023, 24, 1078−1102

Table 6. Studies of $CaCO_3$ Nucleation onto Chitosan in the Presence of Identified Macromolecules

Substrate (with chitosan)	$CaCO_3$ Polymorph and Morphology	Method and Notes	Reference
PAA[a]	All common polymorphs and numerous morphologies	All qualitative, majority gas diffusion method	See Table S4
Poly(Asp)	Calcite, aragonite, vaterite, thin films with circular symmetry	Qualitative, gas diffusion method, % calcite decreased as [poly(Asp)] increased	Sugawara and Kato (2000)[161]
Poly(Asp) and Mg^{2+}	Aragonite, 95% Calcite, 5% Smooth films		
Poly(Asp)	Aragonite, 55%	Qualitative, gas diffusion method	Sugawara and Kato (2004)[162]
Poly(Asp) and Mg^{2+} (Mg/Ca = 6)	Aragonite, 99%		
Poly(Asp)	Aragonite and vaterite, disk-like thin films, (001) orientation	Qualitative, gas diffusion method, % vaterite increased as [poly(Asp)] increased, aragonite disks smaller than vaterite disks	Sugawara et al. (2006)[163]
Poly(Glu)	Vaterite/calcite	Qualitative, gas diffusion, sphere of chitosan coated in poly(Glu)	Tanimoto et al. (2019)[164]
Poly(Glu)	Calcite, thin film	Qualitative, gas diffusion method	Kato et al. (1998)[165]
DNA from salmon sperm	Spherical calcite		
Regenerated silk-fibroin (low conc.)	Ellipsoidal vaterite, irregular calcite	Qualitative, direct mixing, effects of pH and temperature on polymorph were more significant when chitosan was present compared to solution alone	Wu et al. (2011)[166]
Regenerated silk-fibroin (high conc.)	Vaterite disks		
Silk-fibroin	Aragonite films	Qualitative, ammonium carbonate method, synthetic nacre	Raut et al. (2020)[167]
rCAP-1-CD[b]	Aragonite, disk-like thin films	Qualitative, gas diffusion method, peptide contains repeating acidic residues at C-terminus (CD-2, CT-3)	Kumagai et al. (2012)[115]
rCAP-1-CT[c]	Aragonite, disk-like thin films		
Acacia gum	Irregular aggregates that transition to rough rhombohedral, then rhombohedral calcite	Qualitative, direct mixing, polymorph evolved with time (15 min, 1 h, 3 days)	Ritchie et al. (2013)[108]
Alginate	Aragonite nanorods	Qualitative, ammonium carbonate method, *c*-axis inhibition	Suzuki et al. (2016)[168]
Chondroitin-4-sulfate	Vaterite, 77% Calcite, 23% Rough spheres	Qualitative, direct mixing	Mihai et al. (2014)[169]
Chitosan/*ι*-carrageenan composite	Amorphous $CaCO_3$ film	Qualitatitve, direct mixing, artificial seawater	Shahlori et al. (2018)[72,170]
Chitosan/CBM[d] woven composite	Thin film calcite	Qualitative, ammonium carbonate method	Vasiliu et al. (2022)[171]
PAMPS[e] and chitosan/CBM woven composite	Calcite composite layer, crystallites 576 Å		
α-Chitin-agar:PEG[f]: glycerin hydrogel (2:1:1)	Calcite	Qualitative, direct mixing, some *α*-chitin crashed out of the *α*-chitin containing hydrogel during mineralization	Cadez et al. (2018)[69]
β-Chitin-agar:PEG:glycerin hydrogel (2:1:1)	Calcite		
Chitosan/PVA[g] hydrogel with embedded carbonic anhydrase nanoflowers	Calcite, rounded rhombohedral	Qualitative, gas diffusion method, produced 2× more $CaCO_3$ than carbonic anhydrase flowers alone	Wen et al. (2020)[172]

[a]Poly(acrylic acid). [b]Altered rCAP-1 with 2 acidic repeat sequences at C-terminus. [c]Altered rCAP-1 with 3 acidic repeat sequences at C-terminus. [d]Cellulose-based material (70:30 wood pulp: cotton). [e]Poly(2-acrylamido-2-methyl-1-propanesulfonic acid). [f]Polyethylene glycol. [g]Poly(vinyl alcohol).

knowledge, none have done so systematically. Investigations of acacia gum,[108] alginate,[168] and chondroitin-4-sulfate[176] produced different polymorphs and morphologies (calcite aggregates, aragonite nanorods, and vaterite spheres, respectively). In addition to the dissimilar experimental methods used, any number of variables could have influenced the reported results, including polysaccharide functionality, charge density, structure, and/or branching.[84,146]

3.3. Common Theme Underlies Needs for Future Studies. While the previous studies of organic matrix and polysaccharide controls on $CaCO_3$ formation provide insights, Tables 1−6 demonstrate that our understanding of the chemical basis for biomineralization is unsatisfactory. Moving forward, experimental advances should meet two requirements. First, studies must employ methodologies that can quantify crystallization rates at controlled solution compositions.[103,146,177,178] Well-characterized solution compositions are necessary to determine the relationship between chemical driving force and crystallization rates and processes.[179,180] This quantitative capability is critical to establishing the thermodynamic and kinetic controls on crystal nucleation (and growth) reactions and thus, the foundational knowledge required for subsequent advances (see Section 5.1). Tables 1−6 attest to the disparate methods that begin with uncharacterized levels of supersaturation which may also evolve over the course of an experiment. Perhaps unsurprisingly, therefore, the kinetics of crystallization are uncharacterized for even the simplest macromolecular systems. An unfortunate outcome is that, without a quantitative and systematic methodology, few

https://doi.org/10.1021/acs.biomac.2c01394
Biomacromolecules 2023, 24, 1078−1102

investigations can be directly compared to build a consistent physical picture.

Second, future studies need a hypothesis-based approach using well-characterized materials that can establish and build upon basic principles. Natural organic matrices may vary in composition, structure of components, binding between components, and in other ways that, if not elucidated, will preclude a foundational understanding (e.g., Section 3.1.1, Table 2). Past studies also document the difficulty of extracting macromolecular constituents that are representative of the original organic matrix components in diverse individual organisms and their corresponding biomineral structures (e.g., Section 2). In addition, compositions of the extracted fractions have been investigated using laboratory-specific procedures that can introduce uncertainties into the composition, thus further inhibiting definitive conclusions.[59−64] As noted previously, many polysaccharides are so structurally complex that ascertaining some structural details (e.g., detailed monosaccharide sequence) may be out of reach, even using the best and most broadly accepted procedures. *In vitro* laboratory studies of how synthetic and derivatized biomaterials impact crystallization have similar limitations. Shortcomings include the need for consistent characterization and reporting of the reactant materials. These issues present challenges to interpreting or comparing literature results.

With advances in biopolymer synthesis, however, it is now possible to prepare macromolecules with tailored compositions and structures.[139,181−184] This capability opens the way to directly testing claims of functional group activity, providing powerful insights into the mechanistic basis of biomineralization control, particularly when combined with complementary theoretical and experimental approaches.

4. RENEWED FOCUS ON ROLES OF CHARGED GROUPS

The observation that sulfated and phosphorylated molecules are widespread and abundant at sites of mineralization raises new questions regarding the influence of charged macromolecules upon $CaCO_3$ mineralization (e.g., Figure 5 and Table S1). Studies have traditionally focused on the carboxyl groups associated with $CaCO_3$ organic matrices, making important contributions. Given that sulfate and phosphate groups can have significant effects on ion binding and ion solvation as structure directing agents,[185−188] the higher charge density of these species may contribute as much as or more than carboxyls to mineralization.

Studies of sulfated or phosphorylated polysaccharides have received relatively little attention, and such studies are especially missing from consideration in chitin and chitosan systems. One investigation of $CaCO_3$ crystallization determined the polymorphs that formed onto a phosphorylated chitin derivative.[109] Using a qualitative electrocrystallization method, a phosphorylated chitin substrate nucleated calcite and vaterite, in contrast with calcite formation on a substrate of indium zinc oxide (control). The authors suggested that phosphorylated chitin acts as a calcite inhibitor because vaterite is a less stable form of calcium carbonate. However, control studies using chitin alone were not reported, so the effect of phosphate moieties was not conclusively demonstrated.

Outside of chitinous systems, notable studies of functional group effects on $CaCO_3$ crystallization highlight directions for which new investigations using chitosan can be designed. Among studies of (biomacromolecular) sulfate and $CaCO_3$ nucleation, those in the presence of sulfated polysaccharides as glycosaminoglycans (GAGs) are prominent. A good example is the sulfate-containing GAGs associated with the $CaCO_3$ crystals that encase the chicken eggshell. All but one of the GAG families are highly sulfated, and all but one have carboxyl groups on every other monosaccharide.[189] Fernandez et al. (2001) proposed that keratan sulfate proteoglycans (sulfated, no carboxyls) guide $CaCO_3$ nucleation during shell formation, while dermatan sulfate proteoglycans (both sulfates and carboxyls) are proposed to regulate subsequent crystal growth and orientation of crystals.[190−192] Using an ammonium carbonate method (*in vitro*), Arias et al. (2002) observed dermatan sulfate nucleated calcite that grew with a columnar morphology consistent with the prismatic form that is observed in eggshells.[190] In contrast, a desulfated dermatan sulfate derivative produced rounded rhombohedral calcite crystallites. Similar observations were reported *in vivo*, when hens treated with sodium chlorate (to inhibit the sulfation of GAGs) produced shells with poor columnar structure.[191] Rather, more spherical $CaCO_3$ crystals were produced; suggesting a crystal growth inhibition or the possible formation of an amorphous intermediate phase.

Anecdotal observations from experimental studies suggest $CaCO_3$ nucleation is regulated by position of charged groups as well as macromolecule composition. In a quantitative study, Manoli and Dalas (2000) calculated the energy barrier to vaterite nucleation onto chondroitin-4-sulfate and chondroitin-6-sulfate using a constant composition method.[177] Chondroitin-6-sulfate, which differs from chondroitin-4-sulfate only by sulfate position, was associated with a significantly higher barrier to nucleation.[177] This is a revealing illustration of how subtle differences in polysaccharide structure can influence crystallization of inorganic materials.

Other clues to how functional groups modulate nucleation have been provided by studies of nonchitinous scaffolds such as surface assembled monolayers (SAMs).[126,178,193,194] These *in vitro* systems are not directly representative of the organic matrix but do provide a quantitative basis for conceptual models and experimental testing. For example, measurements of $CaCO_3$ nucleation onto a series of SAMs prepared to contain a series of different functional groups, showed rates were dependent upon the functional group chemistry and length of the carbon chains that comprised the monolayer.[178]

Cooperative interactions between charged biopolymer functional groups are a frontier area that will require complementary experimental and computational approaches. Nielsen et al. (2020)[126] investigated the effect of functional group interactions on $CaCO_3$ nucleation using a amphiphilic diblock-polypeptoid where the hydrophilic block contains carboxyl- and amine-functionalized residues. They showed the peptoid substrate presented a significantly lower barrier to nucleation than carboxyl or amine terminated SAMs alone. The barrier to nucleation was still higher on a 1:1 carboxyl:amine-functionalized SAM, illustrating the significance of macromolecular conformation.[126] Similar evidence of cooperative interactions between functional groups is also reported in studies of silica crystallization, where carboxyl and amine groups promote the formation of amorphous silica (Figure 13).[195]

Another example is seen in the *in vitro* experiments of Addadi et al. (1987) where polystyrene films were sulfonated and coated with poly(aspartic acid) or proteins extracted from

https://doi.org/10.1021/acs.biomac.2c01394
Biomacromolecules 2023, 24, 1078−1102

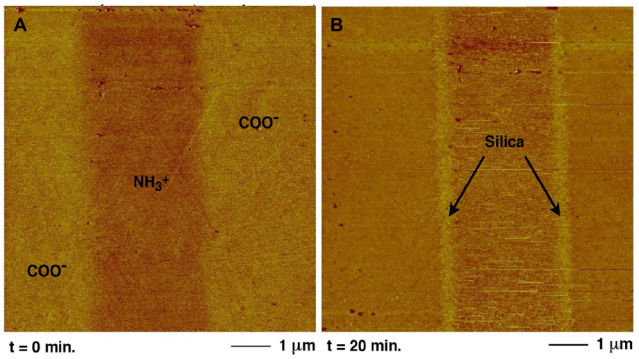

Figure 13. Cooperative interactions of carboxyl- and amine-patterned surfaces (A, before treatment) promote amorphous silica nucleation at the interface of NH_3^+/COO^- groups (B) and demonstrate the potential to control mineral placement through the distribution of functional groups. Reproduced from Wallace et al. (2009)[195] with permission from the American Chemical Society.

the mollusk, *M. californianus*.[196] The sulfonated films increasingly promoted calcite nucleation for up to ten hours of treatment, beyond which they led to decreased crystal nucleation compared to the nonsulfonated control. The average extent of $CaCO_3$ nucleation was directly correlated with the level of sulfonation with or without additional proteins. In contrast, polystyrene sulfonate is reported to nucleate ACC in solution.[197]

When extracted proteins from *M. californianus* were added, the amount of calcite precipitation, and the proportion of crystals with a (001)-preferred orientation, dramatically increased. In further work, the relative influences and interactions between carboxyl and sulfate groups upon $CaCO_3$ nucleation were investigated by cross-linking the proteins of the mollusk organic matrix to tie up their carboxyl groups.[196] These conditions dramatically decreased $CaCO_3$ precipitation and the degree of (001)-dominated orientation, indicating a cooperative effect between sulfates and carboxyls in the native matrix. The evidence suggests that the rate of $CaCO_3$ nucleation onto functionalized materials generally correlates with the average charge density of the functional groups,[146,178] enhanced by cooperative interactions between charged groups.[195,196] This is further related to binding strength.[178,198] Arias et al. (2002, 2004) hypothesize that carboxyl-sulfate interactions change polymer morphology, in turn changing Ca^{2+} binding.[190,192] The highlighted studies above demonstrate the potential to harness crystal patterning in systems by controlling the type and distribution of functional groups.

5. CHITOSAN HYDROGELS AS CANVAS FOR STUDIES OF $CACO_3$ NUCLEATION

Recent advances in polysaccharide hydrogel synthesis, combined with quantitative approaches to investigating crystal nucleation, present new opportunities to conduct hypothesis-based studies of mineralization. Using chitosan as a figurative canvas, it is now possible to prepare hydrogels with tailored and characterized compositions.[182,199−202] Broadly defined, hydrogels are composed of water-soluble polymers that are cross-linked to form networks that are hydrophilic, but insoluble due to their very high effective molecular weights. Many examples of hydrogels are found in natural settings, including the organic matrix. The ability to modify chitosan has advanced significantly in recent years, building upon the previously successful chemoselective modification of alginates and selective oxidation of polysaccharides as components of self-healing hydrogels.[183,203−206]

Chitosan presents multiple options for derivatization due to the different chemistries present at the C2, C3, and C6 carbons of each monosaccharide (e.g., Figure 6B). At near-neutral pH, the C2 amine is more nucleophilic than the hydroxyl groups. On the other hand, the C2 amine is cationic at a low pH (pK_a ca. 6). The primary alcohol C6-OH is less hindered than the other positions, and the secondary C3-OH is the least nucleophilic, providing some selectivity between positions.[207,208] These differences in positional reactivity are not typically sufficient to provide direct and complete regioselectivity in derivatization; however, with certain sterically demanding protecting groups, they can allow highly regioselective reactions. Well-planned and coordinated use of protection and derivatization reactions can force what normally would be an indiscriminate reaction to occur in only one position.[208] A recent review of many chitosan derivatives pertinent to biomedical applications highlights many opportunities for making new synthetic materials.[209] Given that chitosan is often biocompatible in various applications in the mammalian body (and can be degraded and cleared from the body), researchers are motivated by the potential to use chitosan in biomedical fields.[39,40,210] $CaCO_3$ is often used as a sacrificial core for drug delivery devices,[164,211] and chitosan-based hydrogels are a promising medical development.[212−215]

Through controlled synthesis of functionalized chitosans, an array of relevant chemical moieties for hypothesis testing can be prepared. Such moieties include carboxyl,[139,216] sulfate,[181,217,218] and phosphate[184,219] species, for which the density and position of attachment can be controlled. Further modifications to investigate cooperative interactions between groups, as well as polymer properties such as the degree of polymerization, also merit investigation by systematic and quantitative approaches.

5.1. Future Directions for Developing Quantitative Models. To illustrate the scientific value of combining the ability to derivatize chitosan (or other macromolecules) and to conduct measurements of crystal nucleation rates, here we introduce classical nucleation theory (CNT). Our intent is to remind the reader of the quantitative kinetic and thermodynamic insights that can be evaluated from rate measurements. A detailed derivation of CNT is found elsewhere.[179,180,220]

Rates of homogeneous or heterogeneous crystal nucleation from aqueous solutions are determined by two energetic parameters. The thermodynamic barrier to nucleation, Δg_c, describes the excess free energy required to create a newly formed phase of critical radius, r_c, and operates in tandem with an effective kinetic barrier related to individual reactions such as desolvation of solute ions and attachment to the forming nucleus (E_a).[221] The steady state rate of crystallization, J_0, has an exponential dependence on both barriers and is given by

$$J_0 = A\exp\left(\frac{-E_a}{k_B T}\right)\exp\left(\frac{-\Delta g_c}{k_B T}\right) \quad (1)$$

where k_B is the Boltzmann constant and T is absolute temperature. A is a prefactor that correlates with the density of possible nucleation sites.[221] Equation 1 can be simplified to contain a single pre-exponential term (A') such that

https://doi.org/10.1021/acs.biomac.2c01394
Biomacromolecules 2023, 24, 1078−1102

$$J_0 = A' \exp\left(\frac{-\Delta g_c}{k_B T}\right) \quad (2)$$

where A' becomes a kinetic factor that includes multiple terms including the barriers to rates of ion desolvation and attachment.[133] CNT and Equation 2 assume crystallization does not involve the formation of intermediate amorphous or cluster phases.[222]

The thermodynamic barrier, Δg_c, is quantified by the expression

$$\Delta g_c = \frac{f\omega^2\gamma^3}{k_B{}^2 T^2 \sigma^2} \quad (3)$$

where F is a crystal nucleus shape factor, ω is the molecular volume of the crystallizing phase, and σ is the chemical driving force to crystallization as given by the supersaturation of the solution. For the calcite polymorph

$$\sigma_{cal} = \ln\left(\frac{a_{Ca^{2+}} a_{CO_3^{2-}}}{K_{sp,cal}}\right) \quad (4)$$

where a_i is the stoichiometric activity of species that form the nucleus, and K_{sp}, is the equilibrium solubility constant (of the phase that crystallizes) at standard temperature and pressure. For a given macromolecule-crystallization system, the net surface free energy barrier to creating a new crystal, γ_{net} (mJ m^{-2}), is a constant characteristic of the system.

Substituting Equation 3 into Equation 2 obtains

$$J_0 = A' \exp\left(\frac{-F\omega^2\gamma_{net}^3}{k_B{}^3 T^3 \sigma^2}\right) \quad (5)$$

Equation 5 can be simplified by defining

$$B = \frac{F\omega^2\gamma_{net}{}^3}{k_B{}^3 T^3} \quad (6)$$

and substituting Equation 6 into 5 obtains the often-seen form

$$J_0 = A' \exp\left(\frac{-B}{\sigma^2}\right) \quad (7)$$

Assuming that F and ω are constant for a given polymorph, and that T and σ are constant for a single experiment, B is proportional to the net interfacial energy contributions to crystal nucleation for a given system.

Transforming Equation 7 obtains a linear expression:

$$\ln J_0 = \ln A' - \frac{B}{\sigma^2} \quad (8)$$

Equation 8 thus predicts the natural logarithm of the rate of crystal nucleation onto a given substrate is linearly dependent on $1/\sigma^2$ at constant temperature with a slope that is proportional to the thermodynamic barrier to creating a new crystallite.

5.2. Insights from Previous Studies Show Potential of This Approach. Two investigations demonstrate how CNT can be used to better understand molecular controls on crystallization. Although the materials used were not hydrogels, the nucleation theory presented in Section 5.1 (and applied in investigations below) can also be applied to hydrogels, and the methods to quantitatively study them can be similar. Each was motivated by evidence from the biomineralization community (including examples cited in this review) that specialized macromolecules in the organic matrix, including proteins[32,223] or polysaccharides,[3,33,224] provide a stereochemical match to direct the organization of solution ions during crystal nucleation.

By preparing a series of SAMs that presented different functional groups to solution (carboxyl, thiol, phosphate, hydroxyl), Hamm et al. (2013) conducted a series of nucleation rate measurements at a constant temperature for variable conditions of σ. As described elsewhere,[126,146,178,221] each experiment maintained a constant σ by using a continuous flow-through method. Rates of $CaCO_3$ nucleation were determined to be strongly dependent upon the functional group chemistry of each SAM and the length of the carbon chains that comprised the monolayer.[178] For a given chain length (C11, C16 chains, which varied the lateral spacing between functional groups), rates were faster onto thiol-functionalized substrates than carboxyl- or phosphate-containing substrates, whereas rates onto hydroxyl-functionalized SAMs we weakly dependent on supersaturation. By fitting Equations 6 and 8 to the data, the authors were able to determine the values of γ_{net} for each substrate.

To understand these findings, dynamic force spectroscopy was used to make parallel measurements and estimate the crystal-substrate binding free energies (ΔG_b) of the functional group moieties, as well as their conformations.[178] The measurements show a linear correlation between γ_{net} and the ΔG_b of the corresponding functional group moieties (Figure 14), thus demonstrating the role of ion binding in regulating

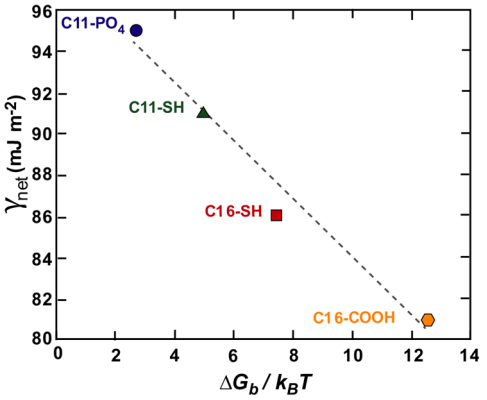

Figure 14. Energy barrier to calcite nucleation (γ_{net}) onto SAM-functionalized surfaces correlates with the free energy of binding (ΔG_b) indicating a lower γ_{net} correlates with stronger binding between calcite and substrate. This relationship is general to all functional group chemistries and conformations (after Hamm et al., 2014).[178]

nucleation.[126] These findings reconcile claims that specialized macromolecules direct nucleation through stereochemical matching with the qualitative "rule of thumb" oft-used by the material science community that biomolecules with strong binding properties are also good nucleators.[34,225−228]

Using a similar experimental approach, Giuffre et al. (2013)[146] determined the nucleation rate of calcite onto chitosan and a series of functionalized polysaccharides at σ values between 5.00 and 5.63 (Figure 15A inset). Again, each experiment maintained a constant σ by using a continuous flow-through method. Fitting Equation 8 to the rate data for each polysaccharide (Figure 15A) and evaluating the slope, they found the energy barrier to $CaCO_3$ nucleation is

https://doi.org/10.1021/acs.biomac.2c01394
Biomacromolecules 2023, 24, 1078−1102

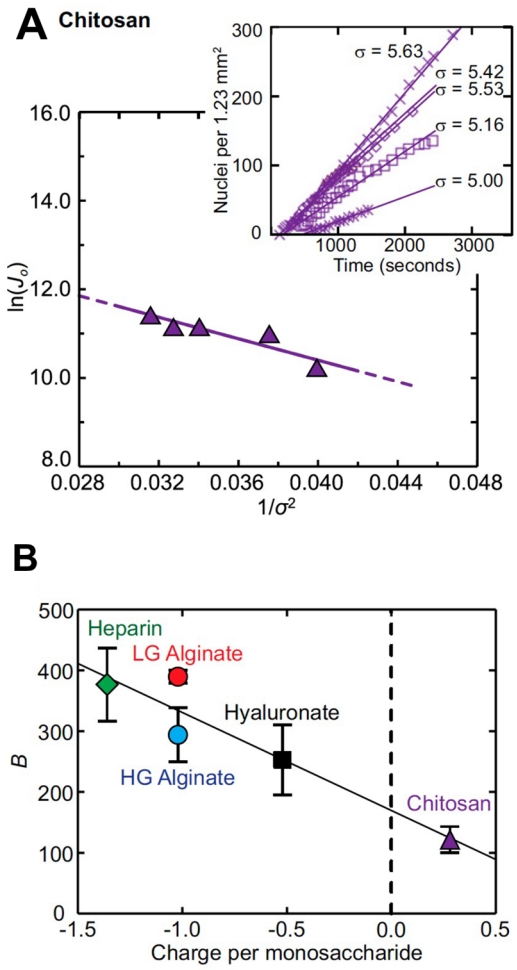

Figure 15. Measurements of calcite nucleation onto a series of polysaccharides quantify rates and interfacial energy barriers. (A) Chitosan nucleation rate (J_0) obeys a linear dependence on supersaturation ($1/\sigma^2$) as predicted by classical nucleation theory (Equation 7). (A, inset) Example of nucleation rates determined for a series of experiments conducted at controlled σ. (B) Slope (B) is polysaccharide dependent where chitosan presents the lowest energy barrier to $CaCO_3$ nucleation compared to other polysaccharides in this study. Assuming terms in B are constant for a given polymorph (Equation 6), B (and thus γ_{net}) is inversely correlated with charge density (per monosaccharide) such that near-neutral polysaccharides present the lowest barriers to calcite formation (after Giuffre et al., 2013).[146]

correlated with polymer composition (Figure 15B). Values of B, and thus γ_{net} (Equation 6) were correlated with net negative charge of the polysaccharide.

The relationship between the energy barrier to calcite nucleation and polysaccharide composition was explained by evaluating the components of γ_{net}. To illustrate, first recall that for a homogeneous system, crystallization is determined by the energy barrier to creating a single type of crystal-water interface (Figure 16A) such that

$$\gamma_{net} = \gamma_{crystal\text{-}water} \quad (9)$$

In contrast, the thermodynamic barrier to crystallization at a macromolecule-water interface is a composite of barriers to forming three interfaces such that γ_{net} is now described by

$$\gamma_{net} = \gamma_{crystal\text{-}water} - h(\gamma_{water\text{-}substrate} - \gamma_{crystal\text{-}substrate}) \quad (10)$$

where h is a factor that depends on the aspect ratio of the crystal nucleus, $\gamma_{water\text{-}substrate}$ is the interfacial energy of the (pre-existing) interface between macromolecule and solution, and $\gamma_{crystal\text{-}substrate}$ is interfacial energy barrier to creating the new crystal interface with the substrate.[220,221]

By making the assumption that $\gamma_{crystal\text{-}water}$ is approximately constant for all experimental conditions, the authors showed that macromolecules with the largest net negative charge (heparin and alginate) are associated with the highest energy barrier to calcite nucleation because of the low $\gamma_{water\text{-}substrate}$. Simply stated, the charged carboxyl and sulfate sites on heparin are hydrophilic and do not easily give up surface waters to create a new crystal-heparin interface. Thus, the thermodynamic barrier to nucleation onto charged substrates is lower than the homogeneous case but still relatively high (Figure 16B).

In contrast, the weaker interactions of water with pure chitosan (compared to highly charged macromolecules) present a lower thermodynamic barrier to nucleation (Figure 16C). This seemingly enigmatic result derives from the larger $\gamma_{water\text{-}substrate}$ for chitosan compared to relatively small shifts in $\gamma_{crystal\text{-}substrate}$ between macromolecules to result in a lower γ_{net} (Equation 9).[146]

Giuffre et al. (2013) also observed a positive correlation between macromolecular charge and the kinetic pre-exponential factor (A').[146] This finding was not fully understood, but a similar relationship was reported for amorphous calcium phosphate (ACP) nucleation onto substrates of amelogenin and amyloid-analog nanoribbons.[133] In this case, a phosphorylated analog presented the highest kinetic prefactor which the authors attributed to the charged groups inducing longer binding times of ions to the surface and/or higher ion exchange rates. The same substrate showed a low γ_{net} to ACP nucleation due to stereochemical matching,[133] raising further questions about the interplay of function group type, density, and position in macromolecules and how these characteristics may regulate ion binding during biomineralization.

The importance of the relationships between macromolecule composition and structure, the γ_{net} of each system, and crystal nucleation rate cannot be overemphasized, yet our understanding is minimal. Nucleation rate depends exponentially on γ_{net} (e.g., Equation 5) and the details of functional composition and structure have tremendous influence on the dynamics (and possibly pathways) of crystal formation. This underlines the importance of understanding solvent-macromolecule interactions and resolving the energetic contributions of each type of interface to build a physical picture of chemical and structural controls on observed nucleation phenomena. The relationships also suggest that there may be multiple ways by which structure-function relationships can be tuned to regulate crystallization onto chitosan and other materials.

6. FUTURE PERSPECTIVES

Looking ahead, chitosan derivatives hold promise for biomineralization research as simple models for natural organic matrices produced by animals and microbes. The ability to tailor the composition to specific degrees and position of substitution confers new opportunities for quantitative studies of relationships between polysaccharide composition and crystal growth. The most powerful is the ability to synthesize and characterize materials that can be used in specifically designed studies for systematic hypothesis testing. Evident in

https://doi.org/10.1021/acs.biomac.2c01394
Biomacromolecules 2023, 24, 1078−1102

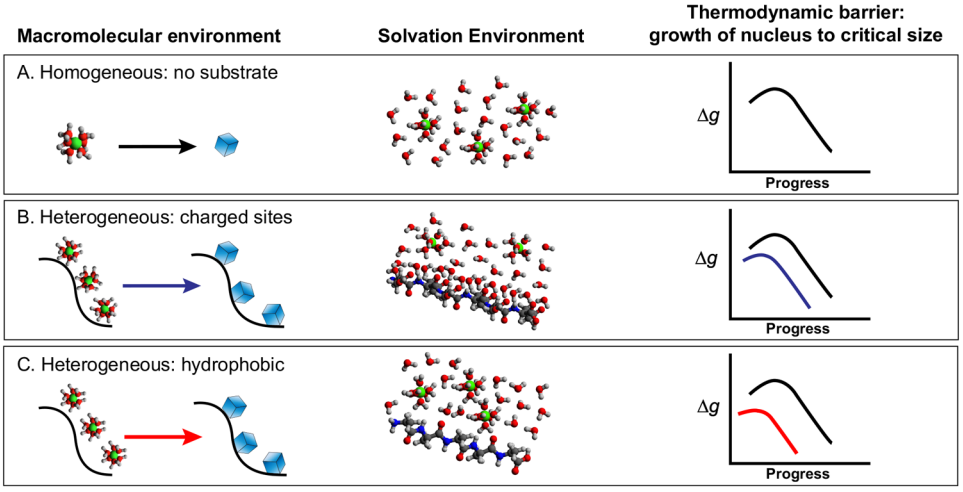

Figure 16. Simplified illustration of relationships between solution environment and the nature of macromolecular substrates in determining rates and energy barriers to crystal nucleation. (A) Homogeneous. In the absence of a substrate, desolvation of the constituent ions en route to forming a crystallite of critical size has a primary control on nucleation rate through $\gamma_{\text{crystal-water}}$ through its control on Δg_c (Equations 3 and 9). (B) Heterogeneous nucleation onto charged macromolecules. Strongly solvated substrates, at localized sites or domains, have a low $\gamma_{\text{water-substrate}}$ which drives γ_{net} to a high value (Equation 10). The primary control of γ_{net} on Δg_c (Equation 3) results in a strong dependence of rate on supersaturation (e.g., Equation 7). (C) Heterogeneous nucleation onto hydrophobic macromolecules (or regions). Weak interactions with water result in a large $\gamma_{\text{water-substrate}}$ and drives γ_{net} to a low value (Equation 10). These environments present the lowest energy barriers to nucleation but are associated with the slowest rates (at high supersaturation).

the discussion of previous studies is the limitation of building a comprehensive understanding from using whatever materials happen to be available. Similar limitations have existed in the availability of commercial products and the highly variable, and typically only partially characterized, natural extracts from the organic matrices of organisms. In contrast, tailored chitinous biomaterials with specified functionality and a series of degree and placement of substitutions will enable systematic studies of the effects of biochemical characteristics on crystallization.

A second opportunity is the ability to deploy quantitative methods to measure nucleation rates and obtain a physical picture of thermodynamic and kinetic relationships. This review has emphasized the influence of functional group chemistry; there are myriad other questions related to the roles of secondary and tertiary structure, regioselectivity, presence of inert electrolytes, local solvent activity, and more. By conducting kinetic studies of crystal nucleation onto suites of characterized materials in tandem with high resolution observational methods, a broader understanding of how macromolecules, or domains within molecular assemblages,[133] modulate mineralization becomes possible.

A third opportunity lies in the power of *in situ* imaging techniques to understand the extent to which the chitosan matrices enhance nucleation through direct binding and organizing ions versus by organizing water and ions in the interfacial region in a way that both lowers the barrier to nucleation and biases the phase that forms. Aqueous solutions are highly structured at mineral interfaces,[229−231] and recent studies suggest the interfacial structure associated with carboxyl functionalized surfaces drives nucleation in the solution near the surface but not on the surface.[232,233] These remarkable findings point to the potential for this mechanism to be generally manifest. The fact that the charge density of such surfaces can be expected to impact the interfacial solution structure suggests a rationale for the correlation between charge density and nucleation kinetics discussed above.

A final opportunity that derives from the first three is the ability to couple quantitative results of these crystallization studies and *in situ* imaging with complementary theoretical modeling[133,234−239] and analytical approaches. It almost goes without saying that computational methods will be integral to future advances.

Such approaches may lead to the ability to regulate the timing and placement of mineralization to form new chitosan-based composite materials. The nontoxic and biodegradable advantages of chitosan and other benign biobased materials make them attractive hosts for crystalline products in novel applications. Possibilities include pharmaceuticals for drug delivery platforms and calcium phosphates for orthopedic and other biomedical applications. Other frontier areas include crystallization-based approaches to patterning "soft" materials and the controlled crystallization of oxides or sulfides within macromolecular matrices for new energy technologies.

■ ASSOCIATED CONTENT

Supporting Information

The Supporting Information is available free of charge at https://pubs.acs.org/doi/10.1021/acs.biomac.2c01394.

Source material for Figure 5 (Table S1), additional chitin-$CaCO_3$ nucleation studies (Table S2), chitosan characterization for papers discussed (Table S3), and studies of $CaCO_3$ nucleation onto chitosan (or chitosan derivatives) in the presence of poly(acrylic acid) (PAA) or onto chitosan derivatives containing PAA (Table S4) (PDF)

■ AUTHOR INFORMATION

Corresponding Author

Patricia M. Dove − *Department of Chemistry, Macromolecules Innovation Institute, Department of Geosciences, and Department of Materials Science and Engineering, Virginia*

https://doi.org/10.1021/acs.biomac.2c01394
Biomacromolecules 2023, 24, 1078−1102

Tech, Blacksburg, Virginia 24061, United States; Email: dove@vt.edu

Authors

Brenna M. Knight − *Department of Chemistry and Department of Geosciences, Virginia Tech, Blacksburg, Virginia 24061, United States;* orcid.org/0000-0002-4400-0067

Kevin J. Edgar − *Department of Sustainable Biomaterials and Macromolecules Innovation Institute, Virginia Tech, Blacksburg, Virginia 24061, United States;* orcid.org/0000-0002-9459-9477

James J. De Yoreo − *Physical Sciences Division, Physical and Computational Sciences Directorate, Pacific Northwest National Laboratory, Richland, Washington 99352, United States; Department of Materials Science and Engineering, University of Washington, Seattle, Washington 98195, United States;* orcid.org/0000-0002-9194-6699

Complete contact information is available at: https://pubs.acs.org/10.1021/acs.biomac.2c01394

Notes

The authors declare no competing financial interest.

■ ACKNOWLEDGMENTS

This project was funded by the US DOE Office of Basic Energy Sciences (OBES), Division of Chemical Sciences, Geosciences and Biosciences through award DE FG02-00ER15112 (to P.M.D.) and its Geosciences Program at PNNL (to J.J.D.Y.) through FWP 56674. PNNL is a multiprogram national laboratory operated for the DOE by Battelle Memorial Institute under Contract DE-AC05-76RL01830. This work was also supported (to K.J.E.) by GlycoMIP, a National Science Foundation Materials Innovation Platform funded through Cooperative Agreement DMR-1933525. We thank C. Sinha for assistance with preparing illustrations and S. Mergelsberg for permitting us to adapt a figure for this publication.

■ REFERENCES

(1) Knoll, A. H. Biomineralization and Evolutionary History. *Rev. Mineral. Geochem.* **2003**, *54* (1), 329−356.

(2) Addadi, L.; Berkovitchyellin, Z.; Weissbuch, I.; Vanmil, J.; Shimon, L. J. W.; Lahav, M.; Leiserowitz, L. Growth and dissolution of organic-crystals with tailor-made inhibitors - implications in stereochemistry and materials science. *Agnew. Chem. Ed. Eng.* **1985**, *24* (6), 466−485.

(3) Mann, S. Molecular recognition in biomineralization. *Nature* **1988**, *332* (6160), 119−124.

(4) Lowenstam, H. A.; Weiner, S. *On Biomineralization*; Oxford University Press: 1989.

(5) Berman, A.; Ahn, D. J.; Lio, A.; Salmeron, M.; Reichert, A.; Charych, D. Total alignment of calcite at acidic polydiacetylene films - cooperativity at the organic-inorganic interface. *Science* **1995**, *269* (5223), 515−518.

(6) Gal, A.; Kahil, K.; Vidavsky, N.; DeVol, R. T.; Gilbert, P. U. P. A.; Fratzl, P.; Weiner, S.; Addadi, L. Particle Accretion Mechanism Underlies Biological Crystal Growth from an Amorphous Precursor Phase. *Adv. Funct. Mater.* **2014**, *24* (34), 5420−5426.

(7) Engel, J. *A Critical Survey of Biomineralization: Control, Mechanisms, Functions and Material Properties*; Springer International Publishing: 2016.

(8) Degens, E. T.; Kazmierczak, J.; Ittekkot, V. Biomineralization and the carbon isotope record. *Tsschermaks Mineral. Petrogr. Mitt.* **1986**, *35* (2), 117−126.

(9) Stojkovic, S.; Beardall, J.; Matear, R. CO2-Concentrating mechanisms in three southern hemisphere strains of emiliania huxleyi. *J. Phycol.* **2013**, *49* (4), 670−679.

(10) Diner, R. E.; Benner, I.; Passow, U.; Komada, T.; Carpenter, E. J.; Stillman, J. H. Negative effects of ocean acidification on calcification vary within the coccolithophore genus Calcidiscus. *Mar. Biol.* **2015**, *162* (6), 1287−1305.

(11) Gilbert, P.; Bergmann, K. D.; Boekelheide, N.; Tambutte, S.; Mass, T.; Marin, F.; Adkins, J. F.; Erez, J.; Gilbert, B.; Knutson, V.; Cantine, M.; Hernandez, J. O.; Knoll, A. H. Biomineralization: Integrating mechanism and evolutionary history. *Sci. Adv.* **2022**, *8* (10), eabl9653.

(12) Currey, J. D. Mechanical-properties of mother of pearl in tension. *Proc. R. Soc. Ser. B, Biol. Sci.* **1977**, *196* (1125), 443−463.

(13) Smith, B. L.; Schaffer, T. E.; Viani, M.; Thompson, J. B.; Frederick, N. A.; Kindt, J.; Belcher, A.; Stucky, G. D.; Morse, D. E.; Hansma, P. K. Molecular mechanistic origin of the toughness of natural adhesives, fibres and composites. *Nature* **1999**, *399* (6738), 761−763.

(14) Wainwright, S. A. Skeletal organization in coral, pocillopora damicornis. *Q. J. Microsc. Sci.* **1963**, *104* (2), 169−183.

(15) Isa, Y.; Okazaki, M. Some observations on the Ca-2+-binding phospholipid from scleractinian coral skeletons. *Comp. Biochem. Physiol. B Biochem. Mol. Biol.* **1987**, *87* (3), 507−512.

(16) Albeck, S.; Weiner, S.; Addadi, L. Polysaccharides of intracrystalline glycoproteins modulate calcite crystal growth in vitro. *Chem. Eur. J.* **1996**, *2* (3), 278−284.

(17) Miyamoto, H.; Miyashita, T.; Okushima, M.; Nakano, S.; Morita, T.; Matsushiro, A. A carbonic anhydrase from the nacreous layer in oyster pearls. *Proc. Natl. Acad. Sci. U. S. A.* **1996**, *93* (18), 9657−9660.

(18) Dauphin, Y. Comparative studies of skeletal soluble matrices from some Scleractinian corals and Molluscs. *Int. J. Biol. Macromol.* **2001**, *28* (4), 293−304.

(19) Cuif, J. P.; Dauphin, Y.; Doucet, J.; Salome, M.; Susini, J. XANES mapping of organic sulfate in three scleractinian coral skeletons. *Geochim. Cosmochim. Acta* **2003**, *67* (1), 75−83.

(20) Miyamoto, H.; Miyoshi, F.; Kohno, J. The carbonic anhydrase domain protein nacrein is expressed in the epithelial cells of the mantle and acts as a negative regulator in calcification in the mollusc Pinctada fucata. *Zool. Sci.* **2005**, *22* (3), 311−315.

(21) Puverel, S.; Tambutte, E.; Pereira-Mouries, L.; Zoccola, D.; Allemand, D.; Tambutte, S. Soluble organic matrix of two Scleractinian corals: Partial and comparative analysis. *Comp. Biochem. Physiol. B* **2005**, *141* (4), 480−487.

(22) Addadi, L.; Joester, D.; Nudelman, F.; Weiner, S. Mollusk shell formation: A source of new concepts for understanding biomineralization processes. *Chem. Eur. J.* **2006**, *12* (4), 980−987.

(23) Kamennaya, N. A.; Ajo-Franklin, C. M.; Northen, T.; Jansson, C. Cyanobacteria as Biocatalysts for Carbonate Mineralization. *Minerals* **2012**, *2* (4), 338−364.

(24) Decho, A. W.; Gutierrez, T. Microbial Extracellular Polymeric Substances (EPSs) in Ocean Systems. *Front. Microbiol.* **2017**, *8*, 922.

(25) Sleight, V. A.; Antczak, P.; Falciani, F.; Clark, M. S. Computationally predicted gene regulatory networks in molluscan biomineralization identify extracellular matrix production and ion transportation pathways. *Bioinformatics* **2020**, *36* (5), 1326−1332.

(26) Marin, F.; Luquet, G.; Marie, B.; Medakovic, D. Molluscan shell proteins: Primary structure, origin, and evolution. In *Current Topics in Developmental Biology*; Schatten, G. P., Ed.; Academic Press: 2008; Vol. *80*, pp 209−276.

(27) Tambutte, S.; Holcomb, M.; Ferrier-Pages, C.; Reynaud, S.; Tambutte, E.; Zoccola, D.; Allemand, D. Coral biomineralization: From the gene to the environment. *J. Exp. Mar. Biol. Ecol.* **2011**, *408* (1−2), 58−78.

(28) Rao, A.; Berg, J. K.; Kellermeier, M.; Gebauer, D. Sweet on biomineralization: effects of carbohydrates on the early stages of calcium carbonate crystallization. *Eur. J. Mineral.* **2014**, *26* (4), 537−552.

(29) Lang, A.; Mijowska, S.; Polishchuk, I.; Fermani, S.; Falini, G.; Katsman, A.; Marin, F.; Pokroy, B. Acidic Monosaccharides become Incorporated into Calcite Single Crystals. *Chem. Eur. J.* **2020**, *26* (70), 16860−16868.
(30) Zhao, Y.; Han, Z.; Yan, H.; Zhao, H.; Tucker, M. E.; Han, M.; Mao, G.; Yin, J. Intracellular and Extracellular Biomineralization Induced by Klebsiella pneumoniae LH1 Isolated from Dolomites. *Geomicrobiol. J.* **2020**, *37* (3), 262−278.
(31) Addadi, L.; Weiner, S. Control and design principles in biological mineralization. *Angew. Chem., Int. Ed.* **1992**, *31* (2), 153−169.
(32) Beniash, E.; Addadi, L.; Weiner, S. Cellular control over spicule formation in sea urchin embryos: A structural approach. *J. Struct. Biol.* **1999**, *125* (1), 50−62.
(33) Chan, C. S.; De Stasio, G.; Welch, S. A.; Girasole, M.; Frazer, B. H.; Nesterova, M. V.; Fakra, S.; Banfield, J. F. Microbial polysaccharides template assembly of nanocrystal fibers. *Science* **2004**, *303* (5664), 1656−1658.
(34) Chung, W. J.; Kwon, K. Y.; Song, J.; Lee, S. W. Evolutionary Screening of Collagen-like Peptides That Nucleate Hydroxyapatite Crystals. *Langmuir* **2011**, *27* (12), 7620−7628.
(35) Sommerdijk, N. A. J. M.; de With, G. Biomimetic CaCO3 mineralization using Designer Molecules and Interfaces. *Chem. Rev.* **2008**, *108* (11), 4499−4550.
(36) George, A.; Ravindran, S. Protein templates in hard tissue engineering. *Nano Today* **2010**, *5* (4), 254−266.
(37) O'Brien, F. J. Biomaterials & scaffolds for tissue engineering. *Mater. Today* **2011**, *14* (3), 88−95.
(38) Asenath-Smith, E.; Li, H.; Keene, E. C.; Seh, Z. W.; Estroff, L. A. Crystal Growth of Calcium Carbonate in Hydrogels as a Model of Biomineralization. *Adv. Funct. Mater.* **2012**, *22* (14), 2891−2914.
(39) Rosellini, E.; Zhang, Y. S.; Migliori, B.; Barbani, N.; Lazzeri, L.; Shin, S. R.; Dokmeci, M. R.; Cascone, M. G. Protein/polysaccharide-based scaffolds mimicking native extracellular matrix for cardiac tissue engineering applications. *J. Biomed. Mater. Res., Part A* **2018**, *106* (3), 769−781.
(40) Pei, B. Y.; Wang, Z. K.; Nie, J. Y.; Hu, Q. L. Highly mineralized chitosan-based material with large size, gradient mineral distribution and hierarchical structure. *Carbohydr. Polym.* **2019**, *208*, 336−344.
(41) Addadi, L.; Weiner, S. Interactions between acidic proteins and crystals - stereochemical requirements in biomineralization. *Proc. Natl. Acad. Sci. U. S. A.* **1985**, *82* (12), 4110−4114.
(42) Linde, A.; Lussi, A.; Crenshaw, M. A. Mineral induction by immobilized polyanionic proteins. *Calcif. Tissue Int.* **1989**, *44* (4), 286−295.
(43) Levi-Kalisman, Y.; Falini, G.; Addadi, L.; Weiner, S. Structure of the Nacreous Organic Matrix of a Bivalve Mollusk Shell Examined in the Hydrated State Using Cryo-TEM. *J. Struct. Biol.* **2001**, *135* (1), 8−17.
(44) Mann, S. *Biomineralization: Principles and Concepts in Bioinorganic Materials Chemistry*; Oxford University Press: 2001.
(45) Weiner, S.; Dove, P. M. An overview of biomineralization processes and the problem of the vital effect. In *Biomineralization*; Dove, P. M., DeYoreo, J. J., Weiner, S., Eds.; Mineralogical Society of America: 2003; Vol. *54*, pp 1−29.
(46) De Yoreo, J. J.; Gilbert, P.; Sommerdijk, N.; Penn, R. L.; Whitelam, S.; Joester, D.; Zhang, H. Z.; Rimer, J. D.; Navrotsky, A.; Banfield, J. F.; Wallace, A. F.; Michel, F. M.; Meldrum, F. C.; Colfen, H.; Dove, P. M. Crystallization by particle attachment in synthetic, biogenic, and geologic environments. *Science* **2015**, *349* (6247), aaa6760.
(47) Qin, W.; Wang, C. Y.; Ma, Y. X.; Shen, M. J.; Li, J.; Jiao, K.; Tay, F. R.; Niu, L. N. Microbe-Mediated Extracellular and Intracellular Mineralization: Environmental, Industrial, and Biotechnological Applications. *Adv. Mater.* **2020**, *32* (22), 1907833.
(48) Young, J. R.; Henriksen, K. Biomineralization within vesicles: The calcite of coccoliths. In *Biomineralization*; Dove, P. M., DeYoreo, J. J., Weiner, S., Eds.; Mineralogical Society of America: 2003; Vol. *54*, pp 189−215.
(49) Taylor, A. R.; Brownlee, C.; Wheeler, G. Coccolithophore Cell Biology: Chalking Up Progress. *Annu. Rev. Mar. Sci.* **2017**, *9*, 283−310.
(50) Kroger, N.; Wetherbee, R. Pleuralins are involved in theca differentiation in the diatom Cylindrotheca fusiformis. *Protist* **2000**, *151* (3), 263−273.
(51) Perry, C. C. Silicification: The processes by which organisms capture and mineralize silica. In *Biomineralization*; Dove, P. M., DeYoreo, J. J., Weiner, S., Eds.; Mineralogical Society of America: 2003; Vol. *54*, pp 291−327.
(52) Hildebrand, M.; Lerch, S. J. L.; Shrestha, R. P. Understanding Diatom Cell Wall Silicification—Moving Forward. *Front. Mar. Sci.* **2018**, *5*, 125.
(53) Mayzel, B.; Aram, L.; Varsano, N.; Wolf, S. G.; Gal, A. Structural evidence for extracellular silica formation by diatoms. *Nat. Commun.* **2021**, *12* (1), 4639.
(54) Lefevre, C. T.; Menguy, N.; Abreu, F.; Lins, U.; Posfai, M.; Prozorov, T.; Pignol, D.; Frankel, R. B.; Bazylinski, D. A. A Cultured Greigite-Producing Magnetotactic Bacterium in a Novel Group of Sulfate-Reducing Bacteria. *Science* **2011**, *334* (6063), 1720−1723.
(55) Rahn-Lee, L.; Komeili, A. The magnetosome model: insights into the mechanisms of bacterial biomineralization. *Front. Microbiol.* **2013**, *4*, 352.
(56) Lin, W.; Zhang, W.; Zhao, X.; Roberts, A. P.; Paterson, G. A.; Bazylinski, D. A.; Pan, Y. Genomic expansion of magnetotactic bacteria reveals an early common origin of magnetotaxis with lineage-specific evolution. *ISME J.* **2018**, *12* (6), 1508−1519.
(57) Banfield, J. F.; Welch, S. A.; Zhang, H. Z.; Ebert, T. T.; Penn, R. L. Aggregation-based crystal growth and microstructure development in natural iron oxyhydroxide biomineralization products. *Science* **2000**, *289* (5480), 751−754.
(58) Penn, R. L.; Zhu, C.; Xu, H.; Veblen, D. R. Iron oxide coatings on sand grains from the Atlantic coastal plain: High-resolution transmission electron microscopy characterization. *Geology* **2001**, *29* (9), 843−846.
(59) Rahman, M. A.; Oomori, T. In Vitro Regulation of CaCO3 Crystal Growth by the Highly Acidic Proteins of Calcitic Sclerites in Soft Coral, Sinularia Polydactyla. *Connect. Tissue Res.* **2009**, *50* (5), 285−293.
(60) Kanold, J. M.; Guichard, N.; Immel, F.; Plasseraud, L.; Corneillat, M.; Alcaraz, G.; Bruemmer, F.; Marin, F. Spine and test skeletal matrices of the Mediterranean sea urchin Arbacia lixula - a comparative characterization of their sugar signature. *Febs J.* **2015**, *282* (10), 1891−1905.
(61) Reggi, M.; Fermani, S.; Samori, C.; Gizzi, F.; Prada, F.; Dubinsky, Z.; Goffredo, S.; Falini, G. Influence of intra-skeletal coral lipids on calcium carbonate precipitation. *CrystEngComm* **2016**, *18* (46), 8829−8833.
(62) Cadez, V.; Skapin, S. D.; Leonardi, A.; Krizaj, I.; Kazazic, S.; Salopek-Sondi, B.; Sondi, I. Formation and morphogenesis of a cuttlebone's aragonite biomineral structures for the common cuttlefish (Sepia officinalis) on the nanoscale: Revisited. *J. Colloid Interface Sci.* **2017**, *508*, 95−104.
(63) Naggi, A.; Torri, G.; Iacomini, M.; Castelli, G. C.; Reggi, M.; Fermani, S.; Dubinsky, Z.; Goffredo, S.; Falini, G. Structure and Function of Stony Coral Intraskeletal Polysaccharides. *ACS Omega* **2018**, *3* (3), 2895−2901.
(64) Rahman, M. A.; Halfar, J.; Adey, W. H.; Nash, M.; Paulo, C.; Dittrich, M. The role of chitin-rich skeletal organic matrix on the crystallization of calcium carbonate in the crustose coralline alga Leptophytum foecundum. *Sci. Rep.* **2019**, *9*, 11869.
(65) Hackman, R. H. Studies on chitin. IV. The occurrence of complexes in which chitin and protein are covalently linked. *Aust. J. Biol. Sci.* **1960**, *13* (4), 568−577.
(66) Falini, G.; Weiner, S.; Addadi, L. Chitin-silk fibroin interactions: Relevance to calcium carbonate formation in invertebrates. *Calcif. Tissue Int.* **2003**, *72* (5), 548−554.
(67) Keene, E. C.; Evans, J. S.; Estroff, L. A. Silk Fibroin Hydrogels Coupled with the n16N-beta-Chitin Complex An in Vitro Organic

https://doi.org/10.1021/acs.biomac.2c01394
Biomacromolecules 2023, 24, 1078−1102

Matrix for Controlling Calcium Carbonate Mineralization. *Cryst. Growth Des.* **2010**, *10* (12), 5169−5175.
(68) Rahman, M. A.; Halfar, J. First evidence of chitin in calcified coralline algae: new insights into the calcification process of Clathromorphum compactum. *Sci. Rep.* **2014**, *4*, 6162.
(69) Čadež, V.; Šegota, S.; Sondi, I.; Lyons, D. M.; Saha, P.; Saha, N.; Sikirić, M. D. Calcium phosphate and calcium carbonate mineralization of bioinspired hydrogels based on β-chitin isolated from biomineral of the common cuttlefish (Sepia officinalis, L.). *J. Polym. Res.* **2018**, *25* (10), 226.
(70) Smetana, K.; Stol, M.; Novak, M.; Daness, J. Influence of carboxylate ions containing polymers on calcification: In vitro study. *Biomaterials* **1996**, *17* (16), 1563−1566.
(71) Zhang, S. K.; Gonsalves, K. E. Influence of the chitosan surface profile on the nucleation and growth of calcium carbonate films. *Langmuir* **1998**, *14* (23), 6761−6766.
(72) Shahlori, R.; McDougall, D. R.; Mata, J. P.; McGillivray, D. J. Effect of acid molecules on biomimetic mineralisation of calcium phosphate and carbonate within biopolymer films using small angle neutron scattering. *Phys. B* **2018**, *551*, 297−304.
(73) Crenshaw, M. A. Inorganic composition of molluscan extrapallial fluid. *Biol. Bull.* **1972**, *143* (3), 506−512.
(74) Weiner, S.; Addadi, L. Acidic macromolecules of mineralized tissues - the controllers of crystal-formation. *Trends Biochem. Sci.* **1991**, *16* (7), 252−256.
(75) Wheeler, A. P.; Low, K. C.; Sikes, C. S. CaCO3 crystal-binding properties of peptides and their influence on crystal-growth. *ACS Symp. Ser.* **1991**, *444*, 72−84.
(76) Weiner, S.; Levi-Kalisman, Y.; Raz, S.; Addadi, L. Biologically formed amorphous calcium carbonate. *Connect. Tissue Res.* **2003**, *44*, 214−218.
(77) Blackwell, J.; Weih, M. A. Structure of chitin-protein complexes - ovipositor of the ichneumon fly megarhyssa. *J. Mol. Biol.* **1980**, *137* (1), 49−60.
(78) Arias, J. L.; Fernandez, M. S. Polysaccharides and Proteoglycans in Calcium Carbonate-based Biomineralization. *Chem. Rev.* **2008**, *108* (11), 4475−4482.
(79) Arroyo-Loranca, R. G.; Hernandez-Saavedra, N. Y.; Hernandez-Adame, L.; Rivera-Perez, C. Ps19, a novel chitin binding protein from Pteria sterna capable to mineralize aragonite plates in vitro. *PLoS One* **2020**, *15* (3), e0230431.
(80) Cornell, B. *Sugar Polymers*. https://ib.bioninja.com.au/standard-level/topic-2-molecular-biology/23-carbohydrates-and-lipids/sugar-polymers.html (accessed October 2020).
(81) Calvert, P. Biomimetic ceramics and composites. *MRS Bull.* **1992**, *17* (10), 37−40.
(82) Whittaker, M. L.; Dove, P. M.; Joester, D. Nucleation on surfaces and in confinement. *MRS Bull.* **2016**, *41* (5), 388−392.
(83) George, P.; Hamid, Z. A.; Zakaria, M. Z. A.; Perimal, E. K.; Bharatham, H. A Short Review on Cockle Shells as Biomaterials in the Context of Bone Scaffold Fabrication. *Sains Malaysiana* **2019**, *48* (7), 1539−1545.
(84) Nielsen, J. W.; Sand, K. K.; Pedersen, C. S.; Lakshtanov, L. Z.; Winther, J. R.; Willemoes, M.; Stipp, S. L. S. Polysaccharide Effects on Calcite Growth: The Influence of Composition and Branching. *Cryst. Growth Des.* **2012**, *12* (10), 4906−4910.
(85) Ibrahim, N. A.; Nada, A. A.; Eid, B. M. *Polysaccharide-Based Polymer Gels and Their Potential Applications*; Springer: Singapore, 2018; pp 97−126.
(86) Bilan, M. I.; Usov, A. I. Polysaccharides of calcareous algae and their effect on the calcification process. *Russ. J. Bioorg. Chem.* **2001**, *27* (1), 2−16.
(87) Rinaudo, M. Chitin and chitosan: Properties and applications. *Prog. Polym. Sci.* **2006**, *31* (7), 603−632.
(88) Muzzarelli, C.; Muzzarelli, R. A. A. Natural and artificial chitosan-inorganic composites. *J. Inorg. Biochem.* **2002**, *92* (2), 89−94.
(89) Chawla, S. P.; Kanatt, S. R.; Sharma, A. K. *Chitosan*; Springer International Publishing: 2015; pp 219−246.
(90) Muzzarelli, R. A. A.; Boudrant, J.; Meyer, D.; Manno, N.; DeMarchis, M.; Paoletti, M. G. Current views on fungal chitin/chitosan, human chitinases, food preservation, glucans, pectins and inulin: A tribute to Henri Braconnot, precursor of the carbohydrate polymers science, on the chitin bicentennial. *Carbohydr. Polym.* **2012**, *87* (2), 995−1012.
(91) Roy, J. C.; Salaün, F.; Giraud, S.; Ferri, A. Solubility of Chitin: Solvents, Solution Behaviors and Their Related Mechanisms. In *Solubility of Polysaccharides*; Zhenbo, X., Ed.; IntechOpen: Rijeka, 2017; p Ch. 7.
(92) Kaya, M.; Mujtaba, M.; Ehrlich, H.; Salaberria, A. M.; Baran, T.; Amemiya, C. T.; Galli, R.; Akyuz, L.; Sargin, I.; Labidi, J. On chemistry of γ-chitin. *Carbohydr. Polym.* **2017**, *176*, 177−186.
(93) Chen, P. Y.; Lin, A. Y. M.; McKittrick, J.; Meyers, M. A. Structure and mechanical properties of crab exoskeletons. *Acta Biomater.* **2008**, *4* (3), 587−596.
(94) Willmer, P. *Invertebrate relationships. Patterns in animal evolution*; Cambridge University: 1990; p, 1−400. i-xiv
(95) Ehrlich, H. Chitin and collagen as universal and alternative templates in biomineralization. *Int. Geol. Rev.* **2010**, *52* (7−8), 661−699.
(96) Raabe, D.; Sachs, C.; Romano, P. The crustacean exoskeleton as an example of a structurally and mechanically graded biological nanocomposite material. *Acta Mater.* **2005**, *53* (15), 4281−4292.
(97) Al-Sawalmih, A.; Li, C.; Siegel, S.; Fabritius, H.; Yi, S.; Raabe, D.; Fratzl, P.; Paris, O. Microtexture and Chitin/Calcite Orientation Relationship in the Mineralized Exoskeleton of the American Lobster. *Adv. Funct. Mater.* **2008**, *18* (20), 3307−3314.
(98) Ogasawara, W.; Shenton, W.; Davis, S. A.; Mann, S. Template Mineralization of Ordered Macroporous Chitin−Silica Composites Using a Cuttlebone-Derived Organic Matrix. *Chem. Mater.* **2000**, *12* (10), 2835−2837.
(99) Kumar, M. A review of chitin and chitosan applications. *React. Funct. Polym.* **2000**, *46* (1), 1−27.
(100) Klinger, C.; Zoltowska-Aksamitowska, S.; Jesionowski, T. Isolation of chitin from aplysina aerophoba using a microwave approach. *Prog. Chem. Appl. Chitin* **2019**, *24*, 61−74.
(101) Klinger, C.; Zoltowska-Aksamitowska, S.; Wysokowski, M.; Tsurkan, M. V.; Galli, R.; Petrenko, I.; Machalowski, T.; Ereskovsky, A.; Martinovic, R.; Muzychka, L.; Smolii, O. B.; Bechmann, N.; Ivanenko, V.; Schupp, P. J.; Jesionowski, T.; Giovine, M.; Joseph, Y.; Bornstein, S. R.; Voronkina, A.; Ehrlich, H. Express Method for Isolation of Ready-to-Use 3D Chitin Scaffolds from Aplysina archeri (Aplysineidae: Verongiida) Demosponge. *Mar. Drugs* **2019**, *17* (2), 131.
(102) Qiao, L. Z.; Zhao, L. S.; Du, K. Construction of hierarchically porous chitin microspheres via a novel Dual-template strategy for rapid and High-capacity removal of heavy metal ions. *Chem. Eng. J.* **2020**, *393*, 124818.
(103) Manoli, F.; Koutsopoulos, S.; Dalas, E. Crystallization of calcite on chitin. *J. Cryst. Growth* **1997**, *182* (1−2), 116−124.
(104) Fernandez, M. S.; Arias, J. I.; Neira-Carrillo, A.; Arias, J. L. Austromegabalanus psittacus barnacle shell structure and proteoglycan localization and functionality. *J. Struct. Biol.* **2015**, *191* (3), 263−271.
(105) Kintsu, H.; Okumura, T.; Negishi, L.; Ifuku, S.; Kogure, T.; Sakuda, S.; Suzuki, M. Crystal defects induced by chitin and chitinolytic enzymes in the prismatic layer of Pinctada fucata. *Biochem. Biophys. Res. Commun.* **2017**, *489* (2), 89−95.
(106) Perez-Huerta, A.; Suzuki, M.; Cappelli, C.; Laiginhas, F.; Kintsu, H. Atom Probe Tomography (APT) Characterization of Organics Occluded in Single Calcite Crystals: Implications for Biomineralization Studies. *C J. Carbon Res.* **2019**, *5* (3), 50.
(107) Kintsu, H.; Perez-Huerta, A.; Ohtsuka, S.; Okumura, T.; Ifuku, S.; Nagata, K.; Kogure, T.; Suzuki, M. Functional analyses of chitinolytic enzymes in the formation of calcite prisms in Pinctada fucata. *Micron* **2021**, *145*, 103063.
(108) Ritchie, A. W.; Watson, M. I. T.; Turnbull, R.; Lu, Z. Z.; Telfer, M.; Gano, J. E.; Self, K.; Greer, H. F.; Zhou, W. Z. Reversed

crystal growth of rhombohedral calcite in the presence of chitosan and gum arabic. *CrystEngComm* **2013**, *15* (47), 10266−10271.
(109) Butto, N.; Cabrera-Barjas, G.; Neira-Carrillo, A. Electrocrystallization of CaCO3 Crystals Obtained through Phosphorylated Chitin. *Crystals* **2018**, *8* (2), 82.
(110) Chen, J. X.; Huang, Y. Q.; Su, M.; Cheng, K.; Zhao, Y. Y. Biomimetic synthesis of oriented aragonite crystals and nacre-like composite material by controlling the fluid type. *Powder Tecnol.* **2016**, *302*, 455−461.
(111) Rodriguez-Navarro, A. B.; Grenier, C.; Checa, A. G.; Jimenez-Lopez, C.; Sanchez-Sanchez, P.; Bertone, D.; Lagos, N. A. Role of the Organic Matter in the Structural Organization of Giant Barnacle Austromegabalanus Psittacus Shell from the Micro- to Nanoscale. *Cryst. Growth Des.* **2021**, *21* (1), 357−365.
(112) Wakayama, H. Hydrothermal Hot Pressing of CaCO3-Chitosan Composites with High CaCO3 Content. *Adv. Mater. Sci. Eng.* **2020**, *2020*, 5908179.
(113) Montroni, D.; Leonard, J.; Rolandi, M.; Falini, G. Morphology and organization of the internal shell of Ariolimax californicus (Gastropoda; Stylommatophora), an asymmetric two-face biomineralized matrix. *J. Struct. Biol.* **2021**, *213* (3), 107764.
(114) Sugawara, A.; Nishimura, T.; Yamamoto, Y.; Inoue, H.; Nagasawa, H.; Kato, T. Self-organization of oriented calcium carbonate/polymer composites: Effects of a matrix peptide isolated from the exoskeleton of a crayfish. *Angew. Chem., Int. Ed.* **2006**, *45* (18), 2876−2879.
(115) Kumagai, H.; Matsunaga, R.; Nishimura, T.; Yamamoto, Y.; Kajiyama, S.; Oaki, Y.; Akaiwa, K.; Inoue, H.; Nagasawa, H.; Tsumoto, K.; Kato, T. CaCO3/Chitin hybrids: recombinant acidic peptides based on a peptide extracted from the exoskeleton of a crayfish controls the structures of the hybrids. *Faraday Discuss.* **2012**, *159*, 483−494.
(116) Suzuki, M.; Saruwatari, K.; Kogure, T.; Yamamoto, Y.; Nishimura, T.; Kato, T.; Nagasawa, H. An Acidic Matrix Protein, Pif, Is a Key Macromolecule for Nacre Formation. *Science* **2009**, *325* (5946), 1388−1390.
(117) Nawarathna, T. H. K.; Nakashima, K.; Kawabe, T.; Mwandira, W.; Kurumisawa, K.; Kawasaki, S. Artificial Fusion Protein to Facilitate Calcium Carbonate Mineralization on Insoluble Polysaccharide for Efficient Biocementation. *ACS Sustainable Chem. Eng.* **2021**, *9* (34), 11493−11502.
(118) Ogawa, T.; Sato, R.; Naganuma, T.; Liu, K.; Sato, S.; Sakaue, S.; Osada, M.; Yoshimi, K.; Muramoto, K. Diversified Biomineralization Roles of Pteria penguin Pearl Shell Lectins as Matrix Proteins. *Int. J. Mol. Sci.* **2021**, *22* (3), 1081.
(119) Levi, Y.; Albeck, S.; Brack, A.; Weiner, S.; Addadi, L. Control over aragonite crystal nucleation and growth: An in vitro study of biomineralization. *Chem. Eur. J.* **1998**, *4* (3), 389−396.
(120) Falini, G.; Albeck, S.; Weiner, S.; Addadi, L. Control of aragonite or calcite polymorphism by mollusk shell macromolecules. *Science* **1996**, *271* (5245), 67−69.
(121) Kato, T.; Suzuki, T.; Irie, T. Layered thin-film composite consisting of polymers and calcium carbonate: A novel organic/inorganic material with an organized structure. *Chem. Lett.* **2000**, *29* (2), 186−187.
(122) Hosoda, N.; Kato, T. Thin-film formation of calcium carbonate crystals: Effects of functional groups of matrix polymers. *Chem. Mater.* **2001**, *13* (2), 688−693.
(123) Munro, N. H.; McGrath, K. M. Biomimetic approach to forming chitin/aragonite composites. *Chem. Commun.* **2012**, *48* (39), 4716−4718.
(124) Munro, N. H.; Green, D. W.; McGrath, K. M. In situ continuous growth formation of synthetic biominerals. *Chem. Commun.* **2013**, *49* (33), 3407−3409.
(125) Mao, L. B.; Gao, H. L.; Yao, H. B.; Liu, L.; Colfen, H.; Liu, G.; Chen, S. M.; Li, S. K.; Yan, Y. X.; Liu, Y. Y.; Yu, S. H. Synthetic nacre by predesigned matrix-directed mineralization. *Science* **2016**, *354* (6308), 107−110.
(126) Nielsen, A. R.; Jelavić, S.; Murray, D.; Rad, B.; Andersson, M. P.; Ceccato, M.; Mitchell, A. C.; Stipp, S. L. S.; Zuckermann, R. N.; Sand, K. K. Thermodynamic and Kinetic Parameters for Calcite Nucleation on Peptoid and Model Scaffolds: A Step toward Nacre Mimicry. *Cryst. Growth Des.* **2020**, *20* (6), 3762−3771.
(127) Inoue, H.; Ohira, T.; Nagasawa, H. Significance of the N- and C-terminal regions of CAP-1, a cuticle calcification-associated peptide from the exoskeleton of the crayfish, for calcification. *Peptides* **2007**, *28* (3), 566−573.
(128) Gower, L. B. Biomimetic Model Systems for Investigating the Amorphous Precursor Pathway and Its Role in Biomineralization. *Chem. Rev.* **2008**, *108* (11), 4551−4627.
(129) Thula, T. T.; Svedlund, F.; Rodriguez, D. E.; Podschun, J.; Pendi, L.; Gower, L. B. Mimicking the Nanostructure of Bone: Comparison of Polymeric Process-Directing Agents. *Polymers* **2011**, *3* (1), 10−35.
(130) Yu, J. G.; Lei, M.; Cheng, B.; Zhao, X. J. Effects of PAA additive and temperature on morphology of calcium carbonate particles. *J. Solid State Chem.* **2004**, *177* (3), 681−689.
(131) Ouhenia, S.; Chateigner, D.; Belkhir, M. A.; Guilmeau, E.; Krauss, C. Synthesis of calcium carbonate polymorphs in the presence of polyacrylic acid. *J. Cryst. Growth* **2008**, *310* (11), 2832−2841.
(132) Nudelman, F.; Pieterse, K.; George, A.; Bomans, P. H. H.; Friedrich, H.; Brylka, L. J.; Hilbers, P. A. J.; de With, G.; Sommerdijk, N. A. J. M. The role of collagen in bone apatite formation in the presence of hydroxyapatite nucleation inhibitors. *Nat. Mater.* **2010**, *9* (12), 1004−1009.
(133) Akkineni, S.; Zhu, C.; Chen, J. J.; Song, M.; Hoff, S. E.; Bonde, J.; Tao, J. H.; Heinz, H.; Habelitz, S.; De Yoreo, J. J. Amyloid-like amelogenin nanoribbons template mineralization via a low-energy interface of ion binding sites. *Proc. Natl. Acad. Sci. U. S. A.* **2022**, *119* (19), e2106965119.
(134) Abo Elsoud, M. M.; El Kady, E. M. Current trends in fungal biosynthesis of chitin and chitosan. *Bull. Natl. Res. Cent.* **2019**, *43* (1), 59.
(135) Kurita, K.; Kamiya, M.; Nishimura, S. I. Solubilization of a rigid polysaccharide - controlled partial n-acetylation of chitosan to develop solubility. *Carbohydr. Polym.* **1991**, *16* (1), 83−92.
(136) Tomihata, K.; Ikada, Y. In vitro and in vivo degradation of films of chitin and its deacetylated derivatives. *Biomaterials* **1997**, *18* (7), 567−575.
(137) Kurita, K. Controlled functionalization of the polysaccharide chitin. *Prog. Polym. Sci.* **2001**, *26* (9), 1921−1971.
(138) Sahariah, P.; Másson, M. Antimicrobial Chitosan and Chitosan Derivatives: A Review of the Structure−Activity Relationship. *Biomacromolecules* **2017**, *18* (11), 3846−3868.
(139) Farion, I. A.; Burdukovskii, V. F.; Kholkhoev, B. C.; Timashev, P. S.; Chailakhyan, R. K. Functionalization of chitosan with carboxylic acids and derivatives of them: Synthesis issues and prospects of practical use: A review. *eXPRESS Polym. Lett.* **2018**, *12* (12), 1081−1105.
(140) Rinaudc, M.; Pavlov, G.; Desbrieres, J. Solubilization of chitosan in strong acid medium. *Int. J. Polym. Anal. Charact.* **1999**, *5* (3), 267−276.
(141) Kubota, N.; Eguchi, Y. Facile preparation of water-soluble N-acetylated chitosan and molecular weight dependence of its water-solubility. *Polym. J.* **1997**, *29* (2), 123−127.
(142) Kubota, N.; Tatsumoto, N.; Sano, T.; Toya, K. A simple preparation of half N-acetylated chitosan highly soluble in water and aqueous organic solvents. *Carbohydr. Res.* **2000**, *324* (4), 268−274.
(143) Qin, C. Q.; Li, H. R.; Xiao, Q.; Liu, Y.; Zhu, J. C.; Du, Y. M. Water-solubility of chitosan and its antimicrobial activity. *Carbohydr. Polym.* **2006**, *63* (3), 367−374.
(144) Xiao, J. W.; Zhu, Y. C.; Liu, Y. Y.; Liu, H. J.; Zeng, Y.; Xu, F. F.; Wang, L. Z. Vaterite selection by chitosan gel: An example of polymorph selection by morphology of biomacromolecules. *Cryst. Growth Des.* **2008**, *8* (8), 2887−2891.
(145) Vasiliu, A. L.; Dinu, M. V.; Zaharia, M. M.; Peptanariu, D.; Mihai, M. In situ CaCO3 mineralization controlled by carbonate

https://doi.org/10.1021/acs.biomac.2c01394
Biomacromolecules 2023, 24, 1078−1102

source within chitosan-based cryogels. *Mater. Chem. Phys.* **2021**, *272*, 125025.
(146) Giuffre, A. J.; Hamm, L. M.; Han, N.; De Yoreo, J. J.; Dove, P. M. Polysaccharide chemistry regulates kinetics of calcite nucleation through competition of interfacial energies. *Proc. Natl. Acad. Sci. U. S. A.* **2013**, *110* (23), 9261−9266.
(147) Fortuna, M. E.; Ungureanu, E.; Jitareanu, C. D. Calcium Carbonate-Carboxymethyl Chitosan Hybrid Materials. *Materials* **2021**, *14* (12), 3336.
(148) Macedo, R.; Marques, N. D.; Paulucci, L. C. S.; Cunha, J. V. M.; Villetti, M. A.; Castro, B. B.; Balaban, R. D. Water-soluble carboxymethylchitosan as green scale inhibitor in oil wells. *Carbohydr. Polym.* **2019**, *215*, 137−142.
(149) Bolivar, G.; Colina, M.; Delgado, B.; Mendizabal, E. The Effect of Carboxymethyl Chitosan on Calcium Carbonate Precipitation in Synthetic Brines. *J. Mex. Chem. Soc.* **2021**, *65* (1), 109−117.
(150) Liang, P.; Shen, Q.; Zhao, Y.; Zhou, Y.; Wei, H.; Lieberwirth, I.; Huang, Y. P.; Wang, D. J.; Xu, D. F. Petunia-shaped superstructures of CaCO3 aggregates modulated by modified chitosan. *Langmuir* **2004**, *20* (24), 10444−10448.
(151) Liang, P.; Zhao, Y.; Shen, Q.; Wang, D. J.; Xu, D. F. The effect of carboxymethyl chitosan on the precipitation of calcium carbonate. *J. Cryst. Growth* **2004**, *261* (4), 571−576.
(152) Yang, X. D.; Xu, G. Y.; Chen, Y. J.; Liu, T.; Mao, H. Z.; Sui, W. P.; Ao, M. Q.; He, F. The influence of O-carboxymethylchitosan on the crystallization of calcium carbonate. *Powder Tecnol.* **2010**, *204* (2−3), 228−235.
(153) Huang, Y. P.; Shen, Q.; Sui, W. P.; Guo, M. L.; Zhao, Y.; Wang, D. J.; Xu, D. F. Peanut-shaped aggregation of CaCO3 crystallites in the presence of an amphiphilic derivative of carboxymethylchitosan. *Colloid Polym. Sci.* **2007**, *285* (6), 641−647.
(154) Yang, X.; Xu, G.; Chen, Y.; Wang, F.; Mao, H.; Sui, W.; Bai, Y.; Gong, H. CaCO3 crystallization control by poly(ethylene oxide)−poly(propylene oxide)−poly(ethylene oxide) triblock copolymer and O-(hydroxy isopropyl) chitosan. *J. Cryst. Growth* **2009**, *311* (21), 4558−4569.
(155) Wang, B. B.; Yang, X. D.; Wang, L.; Li, G. H.; Li, Y. Facile preparation of CaCO3 with diversified patterns modulated by N- (2-hydroxyl)-propyl-3-trimethylammonium chitosan chloride. *Powder Tecnol.* **2016**, *299*, 51−61.
(156) Guo, X. R.; Qiu, F. X.; Dong, K.; Zhou, X.; Qi, J.; Zhou, Y.; Yang, D. Y. Preparation, characterization and scale performance of scale inhibitor copolymer modification with chitosan. *J. Indust. Eng. Chem.* **2012**, *18* (6), 2177−2183.
(157) Maher, Y. A.; Ali, M. E. A.; Salama, H. E.; Sabaa, M. W. Preparation, characterization and evaluation of chitosan biguanidine hydrochloride as a novel antiscalant during membrane desalination process. *Arabian J. Chem.* **2020**, *13* (1), 2964−2981.
(158) Chen, Z. X.; Li, X. X.; Zheng, B. Y. Can Spherical Vaterite Be Biomimetic Synthesized by Using Histidine-Grafted-Chitosan as an Organic Matrix? *J. Inorg. Organomet. Polym. Mater.* **2017**, *27* (4), 1014−1021.
(159) Neira-Carrillo, A.; Yazdani-Pedram, M.; Retuert, J.; Diaz-Dosque, M.; Gallois, S.; Arias, J. L. Selective crystallization of calcium salts by poly (acrylate)-grafted chitosan. *J. Colloid Interface Sci.* **2005**, *286* (1), 134−141.
(160) Neira-Carrillo, A.; Mercade-Jaque, P.; Diaz-Dosque, M.; Tapia-Villanueva, C.; Yazdani-Pedram, M. Influence of Chitosan Grafted Poly(vinyl Sulfonic Acid) as Template on the Calcium Carbonate Crystallization. *J. Iran. Chem. Soc.* **2011**, *8* (3), 811−824.
(161) Sugawara, A.; Kato, T. Aragonite CaCO3 thin-film formation by cooperation of Mg2+ and organic polymer matrices. *Chem. Commun.* **2000**, No. 6, 487−488.
(162) Sugawara, A.; Kato, T. Calcium carbonate/polymer composites: polymorph control for aragonite. *Compos. Interfaces* **2004**, *11* (4), 287−295.
(163) Sugawara, A.; Oichi, A.; Suzuki, H.; Shigesato, Y.; Kogure, T.; Kato, T. Assembled structures of nanocrystals in polymer/calcium carbonate thin-film composites formed by the cooperation of chitosan and poly(aspartate). *J. Polym. Sci., Part A* **2006**, *44* (17), 5153−5160.
(164) Tanimoto, S.; Nishii, I.; Kanaoka, S. Biomineralization-inspired fabrication of chitosan/calcium carbonates core-shell type composite microparticles as a drug carrier. *Int. J. Biol. Macromol.* **2019**, *129*, 659−664.
(165) Kato, T.; Suzuki, T.; Amamiya, T.; Irie, T.; Komiyama, M.; Yui, H. Effects of macromolecules on the crystallization of CaCO3 the Formation of Organic/Inorganic Composites. *Supramol. Sci.* **1998**, *5* (3), 411−415.
(166) Wu, Y.; Cheng, C.; Yao, J.; Chen, X.; Shao, Z. Crystallization of Calcium Carbonate on Chitosan Substrates in the Presence of Regenerated Silk Fibroin. *Langmuir* **2011**, *27* (6), 2804−2810.
(167) Raut, H. K.; Schwartzman, A. F.; Das, R.; Liu, F.; Wang, L. F.; Ross, C. A.; Fernandez, J. G. Tough and Strong: Cross-Lamella Design Imparts Multifunctionality to Biomimetic Nacre. *ACS Nano* **2020**, *14* (8), 9771−9779.
(168) Suzuki, M.; Oaki, Y.; Imai, H. Aragonite Nanorod Arrays through Molecular Controlled Growth on Single-Crystalline Substrate and Polysaccharide Surface. *Cryst. Growth Des.* **2016**, *16* (7), 3741−3747.
(169) Mihai, M.; Schwarz, S.; Doroftei, F.; Simionescu, B. C. Calcium Carbonate/Polymers Microparticles Tuned by Complementary Polyelectrolytes as Complex Macromolecular Templates. *Cryst. Growth Des.* **2014**, *14* (11), 6073−6083.
(170) Shahlori, R.; McDougall, D. R.; Waterhouse, G. I. N.; Yao, F. H.; Mata, J. P.; Nelson, A. R. J.; McGillivray, D. J. Biomineralization of Calcium Phosphate and Calcium Carbonate within Iridescent Chitosan/Iota-Carrageenan Multilayered Films. *Langmuir* **2018**, *34* (30), 8994−9003.
(171) Vasiliu, A. L.; Zaharia, M. M.; Bazarghideanu, M. M.; Rosca, I.; Peptanariu, D.; Mihai, M. Hydrophobic Composites Designed by a Nonwoven Cellulose-Based Material and Polymer/CaCO3 Patterns with Biomedical Applications. *Biomacromolecules* **2022**, *23*, 89−99.
(172) Wen, H.; Zhang, L.; Du, Y. J.; Wang, Z. Y.; Jiang, Y. H.; Bian, H. J.; Cui, J. D.; Jia, S. R. Bimetal based inorganic-carbonic anhydrase hybrid hydrogel membrane for CO2 capture. *J. CO2 Util.* **2020**, *39*, 101171.
(173) Li, Y. D.; Ping, H.; Zou, Z. Y.; Xie, J. J.; Wang, W. M.; Wang, K.; Fu, Z. Y. Bioprocess-inspired synthesis of multilayered chitosan/CaCO3 composites with nacre-like structures and high mechanical properties. *J. Mater. Chem. B* **2021**, *9* (28), 5691−5697.
(174) Wada, N.; Suda, S.; Kanamura, K.; Umegaki, T. Formation of thin calcium carbonate films with aragonite and vaterite forms coexisting with polyacrylic acids and chitosan membranes. *J. Colloid Interface Sci.* **2004**, *279* (1), 167−174.
(175) Payne, S. R.; Heppenstall-Butler, M.; Butler, M. F. Formation of Thin Calcium Carbonate Films on Chitosan Biopolymer Substrates. *Cryst. Growth Des.* **2007**, *7* (7), 1262−1276.
(176) Mihai, M.; Schwarz, S.; Simon, F. Nonstoichiometric Polyelectrolyte Complexes Versus Polyanions as Templates on CaCO3-Based Composite Synthesis. *Cryst. Growth Des.* **2013**, *13* (7), 3144−3153.
(177) Manoli, F.; Dalas, E. Spontaneous precipitation of calcium carbonate in the presence of chondroitin sulfate. *J. Cryst. Growth* **2000**, *217* (4), 416−421.
(178) Hamm, L. M.; Giuffre, A. J.; Han, N.; Tao, J.; Wang, D.; De Yoreo, J. J.; Dove, P. M. Reconciling disparate views of template-directed nucleation through measurement of calcite nucleation kinetics and binding energies. *Proc. Natl. Acad. Sci. U. S. A.* **2014**, *111* (4), 1304−1309.
(179) Nielsen, A. E. *Kinetics of precipitation*; Pergamon Press [distributed in the Western Hemisphere by Macmillan, New York]: Oxford; New York, 1964.
(180) Chernov, A. *Modern Crystallography III: Crystal Growth*; Springer: Berlin, 1984; Vol. 36.
(181) Bedini, E.; Laezza, A.; Parrilli, M.; Iadonisi, A. A review of chemical methods for the selective sulfation and desulfation of polysaccharides. *Carbohydr. Polym.* **2017**, *174*, 1224−1239.

https://doi.org/10.1021/acs.biomac.2c01394
Biomacromolecules 2023, 24, 1078−1102

(182) Chen, J.; Nichols, B. L. B.; Norris, A. M.; Frazier, C. E.; Edgar, K. J. All-Polysaccharide, Self-Healing Injectable Hydrogels Based on Chitosan and Oxidized Hydroxypropyl Polysaccharides. *Biomacromolecules* **2020**, *21* (10), 4261−4272.
(183) Nichols, B. L. B.; Chen, J.; Mischnick, P.; Edgar, K. J. Selective Oxidation of 2-Hydroxypropyl Ethers of Cellulose and Dextran: Simple and Efficient Introduction of Versatile Ketone Groups to Polysaccharides. *Biomacromolecules* **2020**, *21* (12), 4835−4849.
(184) Xia, S. L.; Zhai, Y. C.; Wang, X.; Fan, Q. R.; Dong, X. Y.; Chen, M.; Han, T. Phosphorylation of polysaccharides: A review on the synthesis and bioactivities. *Int. J. Biol. Macromol.* **2021**, *184*, 946−954.
(185) O'Brien, J. T.; Prell, J. S.; Bush, M. F.; Williams, E. R. Sulfate Ion Patterns Water at Long Distance. *J. Am. Chem. Soc.* **2010**, *132* (24), 8248−8249.
(186) Sharma, B.; Chandra, A. Ab Initio Molecular Dynamics Simulation of the Phosphate Ion in Water: Insights into Solvation Shell Structure, Dynamics, and Kosmotropic Activity. *J. Phys. Chem. B* **2017**, *121* (46), 10519−10529.
(187) Teasdale, I. Stimuli-Responsive Phosphorus-Based Polymers. *Eur. J. Inorg. Chem.* **2019**, *2019* (11−12), 1445−1456.
(188) Roy, R.; Jonniya, N. A.; Kar, P. Effect of Sulfation on the Conformational Dynamics of Dermatan Sulfate Glycosaminoglycan: A Gaussian Accelerated Molecular Dynamics Study. *J. Phys. Chem. B* **2022**, *126* (21), 3852−3866.
(189) Gandhi, N. S.; Mancera, R. L. The Structure of Glycosaminoglycans and their Interactions with Proteins. *Chem. Biol. Drug Des.* **2008**, *72* (6), 455−482.
(190) Arias, J. I.; Jure, C.; Wiff, J. P.; Fernandez, M. S.; Fuenzalida, V.; Arias, J. L. In Effect of sulfate content of biomacromolecules on the crystallization of calcium carbonate. *Symposia on Physical Characterization of Biological Materials and Systems/Polymeric Biomaterials for Tissue Engineering/BioInspired Materials-Moving Toward Complexity*, Boston, MA, Nov. 26−29; Boston, MA, 2001; pp 243−248.
(191) Fernandez, M. S.; Moya, A.; Lopez, L.; Arias, J. L. Secretion pattern, ultrastructural localization and function of extracellular matrix molecules involved in eggshell formation. *Matrix Biol.* **2001**, *19* (8), 793−803.
(192) Arias, J. L.; Neira-Carrillo, A.; Arias, J. I.; Escobar, C.; Bodero, M.; David, M.; Fernandez, M. S. Sulfated polymers in biological mineralization: a plausible source for bio-inspired engineering. *J. Mater. Chem.* **2004**, *14* (14), 2154−2160.
(193) Aizenberg, J.; Black, A. J.; Whitesides, G. H. Oriented growth of calcite controlled by self-assembled monolayers of functionalized alkanethiols supported on gold and silver. *J. Am. Chem. Soc.* **1999**, *121* (18), 4500−4509.
(194) Aizenberg, J.; Black, A. J.; Whitesides, G. M. Control of crystal nucleation by patterned self-assembled monolayers. *Nature* **1999**, *398* (6727), 495−498.
(195) Wallace, A. F.; DeYoreo, J. J.; Dove, P. M. Kinetics of Silica Nucleation on Carboxyl- and Amine-Terminated Surfaces: Insights for Biomineralization. *J. Am. Chem. Soc.* **2009**, *131* (14), 5244−5250.
(196) Addadi, L.; Moradian, J.; Shay, E.; Maroudas, N. G.; Weiner, S. A chemical model for the cooperation of sulfates and carboxylates in calcite crystal nucleation: Relevance to biomineralization. *Proc. Natl. Acad. Sci. U. S. A.* **1987**, *84* (9), 2732−2736.
(197) Smeets, P. J. M.; Cho, K. R.; Kempen, R. G. E.; Sommerdijk, N. A. J. M.; De Yoreo, J. J. Calcium carbonate nucleation driven by ion binding in a biomimetic matrix revealed by in situ electron microscopy. *Nat. Mater.* **2015**, *14* (4), 394−399.
(198) Friddle, R. W.; Noy, A.; De Yoreo, J. J. Interpreting the widespread nonlinear force spectra of intermolecular bonds. *Proc. Natl. Acad. Sci. U. S. A.* **2012**, *109* (34), 13573−13578.
(199) Kufelt, O.; El-Tamer, A.; Sehring, C.; Meissner, M.; Schlie-Wolter, S.; Chichkov, B. N. Water-soluble photopolymerizable chitosan hydrogels for biofabrication via two-photon polymerization. *Acta Biomater.* **2015**, *18*, 186−195.
(200) Hamedi, H.; Moradi, S.; Hudson, S. M.; Tonelli, A. E. Chitosan based hydrogels and their applications for drug delivery in wound dressings: A review. *Carbohydr. Polym.* **2018**, *199*, 445−460.
(201) Pakdel, P. M.; Peighambardoust, S. J. Review on recent progress in chitosan-based hydrogels for wastewater treatment application. *Carbohydr. Polym.* **2018**, *201*, 264−279.
(202) Pella, M. C. G.; Lima-Tenorio, M. K.; Neto, E. T. T.; Guilherme, M. R.; Muniz, E. C.; Rubira, A. F. Chitosan-based hydrogels: From preparation to biomedical applications. *Carbohydr. Polym.* **2018**, *196*, 233−245.
(203) Pawar, S. N.; Edgar, K. J. Chemical Modification of Alginates in Organic Solvent Systems. *Biomacromolecules* **2011**, *12* (11), 4095−4103.
(204) Pawar, S. N.; Edgar, K. J. Alginate derivatization: A review of chemistry, properties and applications. *Biomaterials* **2012**, *33* (11), 3279−3305.
(205) Wei, Z.; Yang, J. H.; Liu, Z. Q.; Xu, F.; Zhou, J. X.; Zrinyi, M.; Osada, Y.; Chen, Y. M. Novel Biocompatible Polysaccharide-Based Self-Healing Hydrogel. *Adv. Funct. Mater.* **2015**, *25* (9), 1352−1359.
(206) Liu, H.; Sui, X.; Xu, H.; Zhang, L.; Zhong, Y.; Mao, Z. Self-Healing Polysaccharide Hydrogel Based on Dynamic Covalent Enamine Bonds. *Macromol. Mater. Eng.* **2016**, *301* (6), 725−732.
(207) Sashiwa, H.; Kawasaki, N.; Nakayama, A.; Muraki, E.; Yamamoto, N.; Aiba, S. Chemical modification of chitosan. 14: Synthesis of water-soluble chitosan derivatives by simple acetylation. *Biomacromolecules* **2002**, *3* (5), 1126−1128.
(208) Kurita, K.; Ikeda, H.; Shimojoh, M.; Yang, J. N-phthaloylated chitosan as an essential precursor for controlled chemical modifications of chitosan: Synthesis and evaluation. *Polym. J.* **2007**, *39* (9), 945−952.
(209) Negm, N. A.; Hefni, H. H. H.; Abd-Elaal, A. A. A.; Badr, E. A.; Abou Kana, M. T. H. Advancement on modification of chitosan biopolymer and its potential applications. *Int. J. Biol. Macromol.* **2020**, *152*, 681−702.
(210) Gong, J.; Zhou, Z.; Hu, X.; Wong, M.-k.; Wong, K.-w.; Du, Z. Self-Assembled Chitosan Nanotemplates for Biomineralization of Controlled Calcite Nanoarchitectures. *ACS Appl. Mater. Interfaces* **2009**, *1* (1), 26−29.
(211) Elbaz, N. M.; Owen, A.; Rannard, S.; McDonald, T. O. Controlled synthesis of calcium carbonate nanoparticles and stimuli-responsive multi-layered nanocapsules for oral drug delivery. *Int. J. Pharm.* **2020**, *574*, 118866.
(212) Yao, K. D.; Peng, T.; Goosen, M. F. A.; Min, J. M.; He, Y. Y. pH-Sensitivity of hydrogels based on complex-forming chitosan - polyether interpenetrating polymer network. *J. Appl. Polym. Sci.* **1993**, *48* (2), 343−354.
(213) Hirano, T.; Shiraishi, H.; Ikejima, M.; Uehara, R.; Hakamata, W.; Nishio, T. Chitin oligosaccharide deacetylase from Shewanella baltica ATCC BAA-1091. *Biosci. Biotechnol. Biochem.* **2017**, *81* (3), 547−550.
(214) Ren, B.; Chen, X.; Du, S.; Ma, Y.; Chen, H.; Yuan, G.; Li, J.; Xiong, D.; Tan, H.; Ling, Z.; Chen, Y.; Hu, X.; Niu, X. Injectable polysaccharide hydrogel embedded with hydroxyapatite and calcium carbonate for drug delivery and bone tissue engineering. *Int. J. Biol. Macromol.* **2018**, *118*, 1257−1266.
(215) Wang, J. W.; Kong, Y.; Liu, F.; Shou, D.; Tao, Y. X.; Qin, Y. Construction of pH-responsive drug delivery platform with calcium carbonate microspheres induced by chitosan gels. *Ceram. Int.* **2018**, *44* (7), 7902−7907.
(216) Yoshimura, T.; Uchikoshi, I.; Yoshiura, Y.; Fujioka, R. Synthesis and characterization of novel biodegradable superabsorbent hydrogels based on chitin and succinic anhydride. *Carbohydr. Polym.* **2005**, *61* (3), 322−326.
(217) Warner, D. T.; Coleman, L. L. Selective sulfonation of amino groups in amino alcohols. *J. Org. Chem.* **1958**, *23* (8), 1133−1135.
(218) Holme, K. R.; Perlin, A. S. Chitosan N-sulfate. A water-soluble polyelectrolyte. *Carbohydr. Res.* **1997**, *302* (1−2), 7−12.

https://doi.org/10.1021/acs.biomac.2c01394
Biomacromolecules 2023, 24, 1078−1102

(219) Jayakumar, R.; Reis, R. L.; Mano, J. F. Chemistry and applications of phosphorylated chitin and chitosan. *e-Polym.* **2006**, *6* (1), 035.
(220) De Yoreo, J. J.; Vekilov, P. G. Principles of Crystal Nucleation and Growth. *Rev. Mineral. Geochem.* **2003**, *54* (1), 57−93.
(221) Hu, Q.; Nielsen, M. H.; Freeman, C. L.; Hamm, L. M.; Tao, J.; Lee, J. R. I.; Han, T. Y. J.; Becker, U.; Harding, J. H.; Dove, P. M.; De Yoreo, J. J. The thermodynamics of calcite nucleation at organic interfaces: Classical vs. non-classical pathways. *Faraday Discuss.* **2012**, *159*, 509−523.
(222) Henzler, K.; Fetisov, E. O.; Galib, M.; Baer, M. D.; Legg, B. A.; Borca, C.; Xto, J. M.; Pin, S.; Fulton, J. L.; Schenter, G. K.; Govind, N.; Siepmann, J. I.; Mundy, C. J.; Huthwelker, T.; De Yoreo, J. J. Supersaturated calcium carbonate solutions are classical. *Sci. Adv.* **2018**, *4* (1), eaao6283.
(223) Weiner, S.; Traub, W. X-ray-Diffraction study of the insoluble organic matrix of mollusk shells. *Febs Lett.* **1980**, *111* (2), 311−316.
(224) Chan, C. S.; Fakra, S. C.; Edwards, D. C.; Emerson, D.; Banfield, J. F. Iron oxyhydroxide mineralization on microbial extracellular polysaccharides. *Geochim. Cosmochim. Acta* **2009**, *73* (13), 3807−3818.
(225) Whaley, S. R.; English, D. S.; Hu, E. L.; Barbara, P. F.; Belcher, A. M. Selection of peptides with semiconductor binding specificity for directed nanocrystal assembly. *Nature* **2000**, *405* (6787), 665−668.
(226) Lee, S. W.; Mao, C. B.; Flynn, C. E.; Belcher, A. M. Ordering of quantum dots using genetically engineered viruses. *Science* **2002**, *296* (5569), 892−895.
(227) Mao, C. B.; Solis, D. J.; Reiss, B. D.; Kottmann, S. T.; Sweeney, R. Y.; Hayhurst, A.; Georgiou, G.; Iverson, B.; Belcher, A. M. Virus-based toolkit for the directed synthesis of magnetic and semiconducting nanowires. *Science* **2004**, *303* (5655), 213−217.
(228) Dai, H. X.; Choe, W. S.; Thai, C. K.; Sarikaya, M.; Traxler, B. A.; Baneyx, F.; Schwartz, D. T. Nonequilibrium synthesis and assembly of hybrid inorganic-protein nanostructures using an engineered DNA binding protein. *J. Am. Chem. Soc.* **2005**, *127* (44), 15637−15643.
(229) Fenter, P.; Sturchio, N. C. Mineral-water interfacial structures revealed by synchrotron X-ray scattering. *Prog. Surf. Sci.* **2004**, *77* (5−8), 171−258.
(230) Fukuma, T.; Garcia, R. Atomic- and Molecular-Resolution Mapping of Solid-Liquid Interfaces by 3D Atomic Force Microscopy. *ACS Nano* **2018**, *12* (12), 11785−11797.
(231) Nakouzi, E.; Stack, A. G.; Kerisit, S.; Legg, B. A.; Mundy, C. J.; Schenter, G. K.; Chun, J.; De Yoreo, J. J. Moving beyond the Solvent-Tip Approximation to Determine Site-Specific Variations of Interfacial Water Structure through 3D Force Microscopy. *J. Phys. Chem. C* **2021**, *125* (2), 1282−1291.
(232) Cheng, Y. W.; Tao, J. H.; Zhu, G. M.; Soltis, J. A.; Legg, B. A.; Nakouzi, E.; De Yoreo, J. J.; Sushko, M. L.; Liu, J. Near surface nucleation and particle mediated growth of colloidal Au nanocrystals. *Nanoscale* **2018**, *10* (25), 11907−11912.
(233) Zhu, G. M.; Sushko, M. L.; Loring, J. S.; Legg, B. A.; Song, M.; Soltis, J. A.; Huang, X. P.; Rosso, K. M.; De Yoreo, J. J. Self-similar mesocrystals form via interface-driven nucleation and assembly. *Nature* **2021**, *590* (7846), 416−422.
(234) Harding, J. H.; Duffy, D. M.; Sushko, M. L.; Rodger, P. M.; Quigley, D.; Elliott, J. A. Computational Techniques at the Organic−Inorganic Interface in Biomineralization. *Chem. Rev.* **2008**, *108* (11), 4823−4854.
(235) Yang, M.; Stipp, S. L. S.; Harding, J. Biological Control on Calcite Crystallization by Polysaccharides. *Cryst. Growth Des.* **2008**, *8* (11), 4066−4074.
(236) Raiteri, P.; Demichelis, R.; Gale, J. D. Chapter One - Development of Accurate Force Fields for the Simulation of Biomineralization. In *Methods in Enzymology*; De Yoreo, J. J., Ed.; Academic Press: 2013; Vol. *532*, pp 3−23.
(237) Stack, A. G.; Gale, J. D.; Raiteri, P. Virtual Probes of Mineral−Water Interfaces: The More Flops, the Better! *Elements* **2013**, *9* (3), 211−216.
(238) Sparks, D. J.; Romero-González, M. E.; El-Taboni, E.; Freeman, C. L.; Hall, S. A.; Kakonyi, G.; Swanson, L.; Banwart, S. A.; Harding, J. H. Adsorption of poly acrylic acid onto the surface of calcite: an experimental and simulation study. *Phys. Chem. Chem. Phys.* **2015**, *17* (41), 27357−27365.
(239) Demichelis, R.; Schuitemaker, A.; Garcia, N. A.; Koziara, K. B.; De La Pierre, M.; Raiteri, P.; Gale, J. D. Simulation of Crystallization of Biominerals. *Annu. Rev. Mater. Res.* **2018**, *48* (1), 327−352.

https://doi.org/10.1021/acs.biomac.2c01394
Biomacromolecules 2023, 24, 1078−1102